"It's Team Work": Multilayered Wear-Resistant and Lubricating Overcoats Derived from the Synergy of Ultrathin Carbon Surface and Interface Chemistry

Rajesh Kumar[1,2], Pankaj Bharti[1,2], Chetna Dhand[1], Reuben J. Yeo[3], Mingsheng Zhang[3], Neeraj Dwivedi[1,2,*]

[1]CSIR-Advanced Materials and Processes Research Institute (AMPRI), Bhopal 462026, India

[2]Academy of Scientific and Innovative Research (AcSIR), Ghaziabad-201002, India

[3]Institute of Materials Research and Engineering (IMRE), Agency for Science, Technology, and Research (A*STAR), 2 Fusionopolis Way, Innovis, 08-03, Singapore 138634, Republic of Singapore

[*]**Email:** neerajdwivedi6@gmail.com and neeraj.dwivedi@ampri.res.in (N. Dwivedi)

Keywords: Ultrathin overcoats, carbon surface chemistry, interface chemistry, lubricity, wear-resistance

Abstract

High friction and wear remain the major concerns in moving mechanical assemblies (MMAs), leading to an excessive amount of wasted energy and premature system failure. While the use of protective overcoats on the moving surfaces is a common solution to overcome these limitations, achieving excellent tribological characteristics at ultrathin overcoat thicknesses remains very challenging. Here, by combining the benefits arising from an enhanced carbon surface and a robust substrate-overcoat interface chemistry, we report the development of tribologically resilient sub-5 nm carbon-based overcoats on mechanically soft metallic alloy substrates which show considerably lower friction and higher wear resistance than commercially grown overcoats. The use of an interlayer coupled with an energetic process for carbon growth not only enhanced the sp^3 carbon bonding content but also promoted interatomic mixing and the formation of hybrid bonds that significantly improved the interfacial strength and hence the substrate-overcoat adhesion, demonstrating excellent wear resistance in a rigorous tribological environment. Moreover, further modifying the overcoat surface with a composite layer of multilayer graphene flakes and multiwall carbon nanotubes was shown to immensely boost the lubricity and wear durability.

1. Introduction

Friction is a largely unavoidable phenomenon that arises from the movement of two surfaces in contact. Throughout history, man has been looking at ways to mitigate the friction generated in mechanical systems to do work [1-5]. High friction is undesirable because it results in huge energy losses, hence lowering productivity and efficiency. In many moving mechanical assemblies (MMAs), it has been reported that about 20-30% energy input into the system is required to overcome friction [1, 6]. In addition, high friction leads to rapid degradation and loss of material due to wear. As such, the development of solutions to reduce friction and wear is crucial to improve the energy efficiency and the durability of MMAs. Just a small reduction in friction and wear could contribute to significant energy savings, extend the working lifetime of the system, reduce the need for parts replacement and disposal, and is thus vital for sustainable technologies.

The hard disk drive (HDD) is one such system where these tribological concerns are prevalent [2, 7]. During a normal read/write operation of the HDD, the hard disk (HD) media, which contains the stored digital data, is spun at high speeds several nanometers below the read head, known as the fly-height[8, 9]. Due to the extremely small fly-height, there are occasions where the read head could come into contact with the fast-spinning disk. Hence, on top of the HD media, which is made up of mechanically soft magnetic layers, a protective carbon overcoat of 2.7-3 nm and a ~ 1-1.2 nm thick perfluoropolyether (PFPE)-based lubricant layer are recently used to reduce the friction, wear and corrosion of the HD media so as to prevent data loss [8-10]. However, the overcoat thickness contributes to the magnetic spacing between the media and the read head [7, 9], and according to Wallace equation [11], the read-back signal weakens exponentially as the magnetic spacing is increased. In recent years, reducing the HD media overcoat thickness has been one of the central subjects of research to attain higher data storage

densities [9, 12]. Ideally, the HD media overcoat should have high hardness and wear resistance, aid in reducing friction and possess excellent barrier properties, even at reduced thicknesses[13, 14]. Given the overcoat thickness constraints for the technological development of high storage density HDDs, tremendous progress has been made to reduce HD media overcoat thickness from 100-150 nm [15] to sub-5 nm until recently [16-18]. To accomplish this, a wide variety of overcoats, such as silicon nitride, ZrO_2, SiO_2, TiSiC, sputtered carbon, carbon nitride, plasma assisted chemical vapor deposition-based hydrogenated carbon (a-CH_x), or a combination of these materials, have been screened[19-27].

Yet, the protective properties of recent commercial overcoats on HD media begs further improvement. The ~2.7-3 nm thick commercial carbon overcoat, with or without a ~ 1-1.2 nm thick perfluoropolyether (PFPE)-based lubricant (total thickness around ~4 nm) have shown moderate friction reduction and suffers from large wear when tested using ball-on-disk tribology [2, 12]. Hence, 3 to 5 nm thick films are quite often investigated for research and feasibility testing of new materials or new technologies. For example, Rajauria *et al.* had investigated ~ 5 nm thick carbon-based overcoats on HD media for high-speed tribology [16]. Jones *et al.* [18] had investigated the thermal stability of ~5 nm carbon overcoat films on hard disk media for heat-assisted magnetic recording (HAMR) and had found oxidation and burning of the overcoats in the tested environment. Lee *et al.* [28] investigated the nanomechanical properties of sub-10 nm overcoats for magnetic storage systems. Wang et al. investigated the thermal stability of 9.4-9.6 nm films under HAMR-like conditions[20]. Scharf *et al.* [29] had reported the mechanical strength and wear resistance of 5 nm thick ion-beam deposited carbon overcoats for HD media. Bernhard *et al.* [30] had also investigated amorphous carbon-based overcoats with thickness up to 10 nm for magnetic storage systems. Recently, Chatarat *et al.* [31] investigated the diamond-like carbon

coatings of thickness up to 5 nm for magnetic storage devices. Thus, there is a need to develop sub-5 nm overcoats that perform better than conventional overcoats, and which could be further reduced to ≤ 2 nm for future ultra-high storage density HDD technologies.

In some MMAs, rigorous tribo-interfaces are formed which could be due to a large contact pressure or load exerted on the sliding body, high sliding speeds, long sliding periods of time, complex surface structures of the sliding surfaces, reactive chemistries of the sliding surfaces, etc. For example, in magnetic tape drives (TDs), the read head is always in contact with the sliding magnetic tape media, and in normal operation, this contact sliding process can continue for a long time at speeds of up to several meters per second [32-35]. Protective overcoats with thicknesses of 10-40 nm have been applied onto the surface of the TD read head to control the friction and wear generated by contact sliding, but most of them have encountered premature failure[32, 33]. Like magnetic HDDs, to develop TDs with ultra-high storage capacities, the thickness of read head overcoat must be reduced to sub-10 nm with similar or better tribological protection, which is very challenging for such a harsh operating environment. Nonetheless, recent efforts have been made to develop sub-10 nm carbon-based overcoats for tape head with good wear durability[32, 36]. Besides TDs, there are many other systems possessing rigorous tribo-interfaces such as turbines, gears, etc., making it very challenging to ensure the persistence of the coatings. While carbon overcoats grown by energetic processes such as ion beam deposition, filtered cathodic vacuum arc (FCVA), etc. have shown great potential for tribological control, even at low thickness and in rigorous tribological scenarios[13, 14, 37], a better understanding of the overcoat's properties and architecture is essential for advancing and developing durable overcoat technologies for next-generation high-performance MMAs.

In this work, we have developed and demonstrated (i) high-performance ultrathin overcoats for HD media, and (ii) ultrathin overcoats for rigorous tribological environments such as TDs, micro/nano-electromechanical systems (MEMS/NEMS), as well as for moving components in large machinery. We show the development of a ~ 2 nm thick amorphous carbon film on HD media grown by an energetic process at 90 eV which demonstrated significantly reduced friction and improved wear durability than a ~2.7 nm thick commercial carbon overcoat with and without a ~1-1.2 nm PFPE lubricant layer. We further engineered the interface of carbon with the introduction of titanium (Ti) and silicon nitride (SiN_x) interlayers to develop interface-enhanced bilayer overcoats that yielded superior tribological behavior, in particular for the Carbon/Ti bilayer overcoats. Further, we also investigated the tribological properties of our overcoats at a higher applied load (3 N) and for longer periods of time (30,000 cycles) in tribological tests to mimic relatively harsh tribological environments. Finally, we attempted to further modify the carbon overcoat surfaces with a composite layer comprising multilayer graphene (G) flakes and multiwall carbon nanotubes (MWCNT), denoted as a GNT composite layer, and compared its performance to a layer of G flakes to further tune the sliding friction and wear properties.

2. Experimental Methods

Monolithic carbon (C), C/Ti bilayer and C/SiN_x bilayer overcoats were prepared on HD media, and these samples were labelled C-M, C-Ti-M and C-SiN_x-M, respectively. The carbon film in these monolithic or bilayer overcoats were deposited at 90 eV by the plasma-based vacuum deposition process. The Ti layer was grown by DC sputtering of a Ti target whereas the SiN_x layer was deposited by RF sputtering of a Si_3N_4 target. Samples of bare HD media (B-M), HD media with a ~ 2.7 nm commercial carbon overcoat (CO-M), and HD media with a ~2.7 nm commercial carbon overcoat and a ~ 1-1.2 nm PFPE lubricant layer (L-CO-M) were included for reference and

comparison purposes. To modify the surfaces of these samples, G or GNT composite layers were applied by spin coating solutions of G or G+MWCNT, respectively, directly onto the samples. The G solution was prepared in isopropyl alcohol (IPA) with a concentration of 1 mg mL^{-1}, while the G+MWCNT hybrid solution was prepared in IPA with a G:MWCNT ratio of 1:1 and an overall concentration of 1 mg mL^{-1}. In total, three sets of samples were studied: one set without further surface modification, one set modified by adding a spin-coated layer of multilayer G flakes, and one set modified by adding a spin-coated GNT composite layer. A detailed description of the samples is presented in Table 1, and cartoons showing the cross-sections of the overcoat layers for all the samples studied in this work are presented in Figures 1a-1r.

The samples were characterized to investigate the thicknesses of the overcoat layers, their chemical bonding environment, and their tribological properties. High resolution transmission electron microscopy (HRTEM) (HRTEM, JEOL JEM2100F) was used to measure the cross-sectional thicknesses of the monolithic and bilayer overcoats. The HRTEM measurements on G and GNT samples was performed on JEOL F200, JAPAN equipment. X-ray photoelectron spectroscopy (XPS, *PHI Quantera SXM Scanning X-ray Microprobe*) measurements were carried out with Al Kα radiation ($h\nu$ = 1486.6 eV) to study the chemical states and compositions within the overcoats and at the interfaces of the overcoat layers. The beam's spot size on the sample was 200 µm × 200 µm, and the pass energy and step size were 224 eV and 0.8 eV respectively for survey scans, and 55 eV and 0.1 eV respectively for the high-resolution scans. The vacuum pressure during the XPS measurements was kept at around 1 x 10^{-8} Torr. Tribological measurements were performed using a rotating ball-on-disk tribometer (*DUCOM, India*) at a relative humidity (RH) of 35 ± 5 %, and temperature of ~25 ºC. Two different loads were used for the tribological tests, a low load of 0.1 N and higher load of 3.0 N. During the test, a 2 mm diameter

sapphire (Al_2O_3) ball was used as the counterface. Tests were run for 6000 rotational cycles lasting approximately 1 h, but a few selected samples were further subjected to longer duration tribological tests that were run for 30000 cycles over a period of 5 h. For the tribological tests run for 6000 cycles, a stable coefficient of friction (COF) value was determined from the more stable friction region between 3600 and 6000 cycles. From at least two to four tribological measurements for each sample, different stable COF values were obtained, and from these values an average stable COF value (denoted simply as average COF) was calculated together with its corresponding standard deviation. After each tribological test, optical images of the sapphire ball's wear scar and the sample's wear track were captured using an optical microscope. Detailed wear examination on a few important samples was carried out by performing XPS high resolution scans inside and outside the wear tracks after the ball-on-disk tribological tests. For these smaller area scans, a spot size of 100 μm × 100 μm was used, along with a pass energy of 55 eV and a step size of 0.1 eV.

3. Results and Discussion

Figures 1s-1u show the cross-sectional HRTEM images of monolithic C, C/Ti and C/SiN_x bilayer overcoats for thickness measurement. In Figure 1s, the thickness of the monolithic C overcoat (sample C-M) was measured to be ~ 2 nm. In Figure 1t, the individual layer thicknesses of C and Ti in the C/Ti bilayer overcoat (sample C-Ti-M) were measured to be ~ 1.7 nm and ~ 2.8 nm, respectively. In Figure 1u, the overall thickness of the C/SiN_x bilayer overcoat (sample C-SiN_x-M) was measured to be ~3.5 nm as the individual C and SiN_x layers could not be easily distinguished from their similar contrast in HRTEM. Nevertheless, from the C thickness measurement of the C/Ti bilayer overcoat in Figure 1t, we deduced the thicknesses of C and SiN_x to be ~ 1.7 nm and ~ 1.8 nm, respectively.

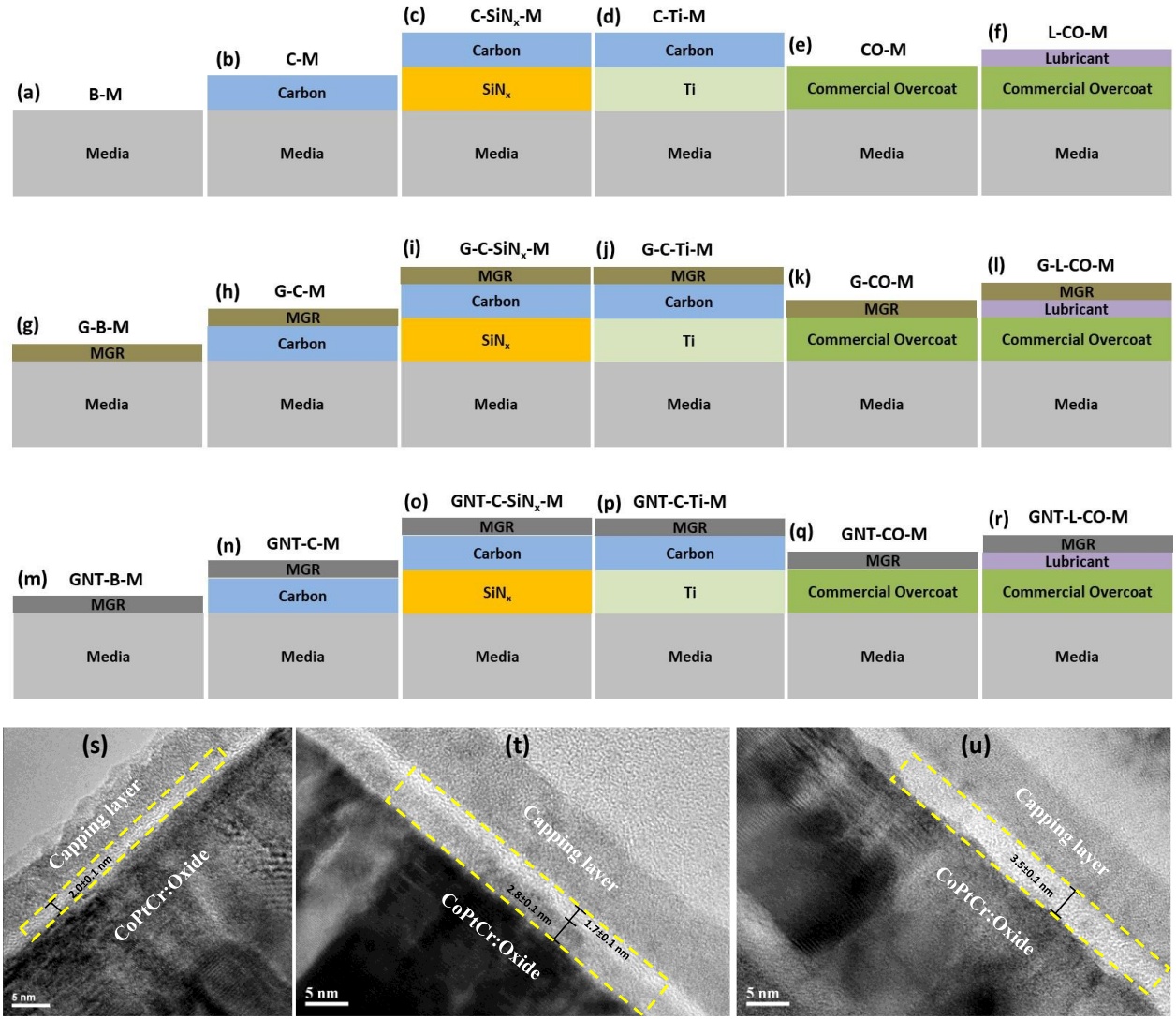

Figure 1: Schematic representations of bare and different carbon-overcoated media samples: (a) B-M sample, (b) C-M, (c) C-SiN_x-M, (d) C-Ti-M, (e) CO-M, (f) L-CO-M. Samples surface-modified with a layer of multilayer graphene flakes (g) G-B-M, (h) G-C-M, (i) G-C-SiN_x-M, (j) G-C-Ti-M, (k) G-CO-M, (l) G-L-CO-M. Samples surface-modified with a composite layer of multilayer graphene and multiwall carbon nanotubes (m) GNT-B-M, (n) GNT-C-M, (o) GNT-C-SiN_x-M, (p) GNT-C-Ti-M, (q) GNT-CO-M, (r) GNT-L-CO-M. HRTEM images of carbon-based overcoats for thickness measurement (s) monolithic carbon, (t) C/Ti and (u) C/SiN_x bilayer overcoats. Scale bars represent 5 nm. Tantalum is used as the capping layer on the samples to provide image contrast in HRTEM imaging.

Table 1: List of different samples used in this work with their detailed descriptions.

Sample Label	Sample Description
B-M	Co-alloy-based commercial hard disk media without any overcoat and lubricant. It is also referred to as bare media.
C-M	Co-alloy-based commercial hard disk media with a carbon overcoat grown at 90 eV. The thickness of carbon measured by HRTEM was ~2 nm.
C-SiN_x-M	Co-alloy-based commercial hard disk media with a carbon/SiN_x bilayer overcoat where the carbon layer was grown at 90 eV. The thickness of carbon measured by HRTEM was ~1.7 nm. The thickness of SiN_x was determined to be ~ 1.8 nm.
C-Ti-M	Co-alloy-based commercial hard disk media with a carbon/Ti bilayer overcoat, where the carbon layer was grown at 90 eV. The thickness of carbon measured by HRTEM was ~1.7 nm while Ti was ~ 2.8 nm.
CO-M	Co-alloy-based commercial hard disk media with a commercial carbon overcoat (~2.7 nm) but without lubricant.
L-CO-M	Co-alloy-based commercial hard disk media with a commercial carbon overcoat (~2.7 nm) and a ~ 1-1.2 nm PFPE lubricant layer.
G-B-M	B-M with a top layer of multilayer graphene flakes.
G-C-M	C-M with a top layer of multilayer graphene flakes.
G-C-SiN_x-M	C-SiN_x-M with a top layer of multilayer graphene flakes.
G-C-Ti-M	C-Ti-M with a top layer of multilayer graphene flakes.
G-CO-M	CO-M with a top layer of multilayer graphene flakes.
G-L-CO-M	L-CO-M with a top layer of multilayer graphene flakes.
GNT-B-M	B-M with a top hybrid layer of multilayer graphene flakes and multiwall carbon nanotubes.
GNT-C-M	C-M with a top hybrid layer of multilayer graphene flakes and multiwall carbon nanotubes.
GNT-C-SiN_x-M	C-SiN_x-M with a top hybrid layer of multilayer graphene flakes and multiwall carbon nanotubes.
GNT-C-Ti-M	C-Ti-M with a top hybrid layer of multilayer graphene flakes and multiwall carbon nanotubes.
GNT-CO-M	CO-M with a top hybrid layer of multilayer graphene flakes and multiwall carbon nanotubes.
GNT-L-CO-M	L-CO-M with a top hybrid layer of multilayer graphene flakes and multiwall carbon nanotubes.

To obtain a deeper insight into the sliding friction and wear properties of the developed overcoats, we performed ball-on-disk tribological tests on the overcoated samples for 6000 cycles. Figure 2a shows the frictional curves depicting the variation of COF with respect to the number of cycles. Figure 2b shows the average COF values for the different samples. Figure 2c displays the

optical images of the balls and the wear tracks for wear analysis of the samples, for the tests conducted at the low normal contact load of 0.1 N. The bare media sample B-M exhibited a high fluctuating friction with average COF of ~ 0.4 and severe wear damage as observed by a wide and intense wear scar on the ball as well as a wide and deep wear track on the sample. The introduction of the commercial carbon overcoat (~ 2.7 nm) without lubricant (sample CO-M) and with lubricant (L-CO-M) marginally improved the tribological properties of the HD media, although high friction with large fluctuations were still observed throughout the test. Even though the average COFs of both samples were lower than B-M, the L-CO-M sample exhibited a large standard deviation in the measured average COF. Furthermore, visible wear was still observed for both CO-M and L-CO-M. Interestingly, the ~ 2 nm thick carbon grown by us at 90 eV (sample C-M) greatly reduced the sliding friction, with its average COF maintained at < 0.3, which indicated more than 25% reduction in friction with respect to B-M. Moreover, sample C-M showed excellent wear resistance as confirmed by the relatively fainter wear track and less debris transferred to the ball as compared to samples B-M, CO-M and L-CO-M. This clearly suggests that the energetically grown ~ 2 nm carbon overcoat in sample C-M achieves better tribological properties than relatively thicker commercially grown overcoats, and could potentially be a game-changer for the advancement of magnetic data storage technology.

SiN_x and Ti interlayers were introduced between the carbon overlayer and the media substrate to further engineer the friction and wear. However, the SiN_x interlayer in sample C-SiN_x-M did not favor a further reduction in friction. Instead, it slightly enhanced the wear of the media/overcoat with respect to the monolithic carbon layer sample C-M. Nevertheless, the tribological performance of the C/SiN_x bilayer overcoat (sample C-SiN_x-M) was found to be superior to the commercially grown overcoats in samples CO-M and L-CO-M, as confirmed by

the relatively lower wear and friction in C-SiN$_x$-M. What is exceptional was that sample C-Ti-M achieved the lowest friction (COF ~ 0.2) out of all the samples tested, almost half of the COF of sample B-M. In addition, it displayed the highest wear resistance amongst all the samples. Thus, the introduction of the Ti interlayer had proved to be effective in further enhancing the tribological performance of the carbon overcoat grown by the energetic process.

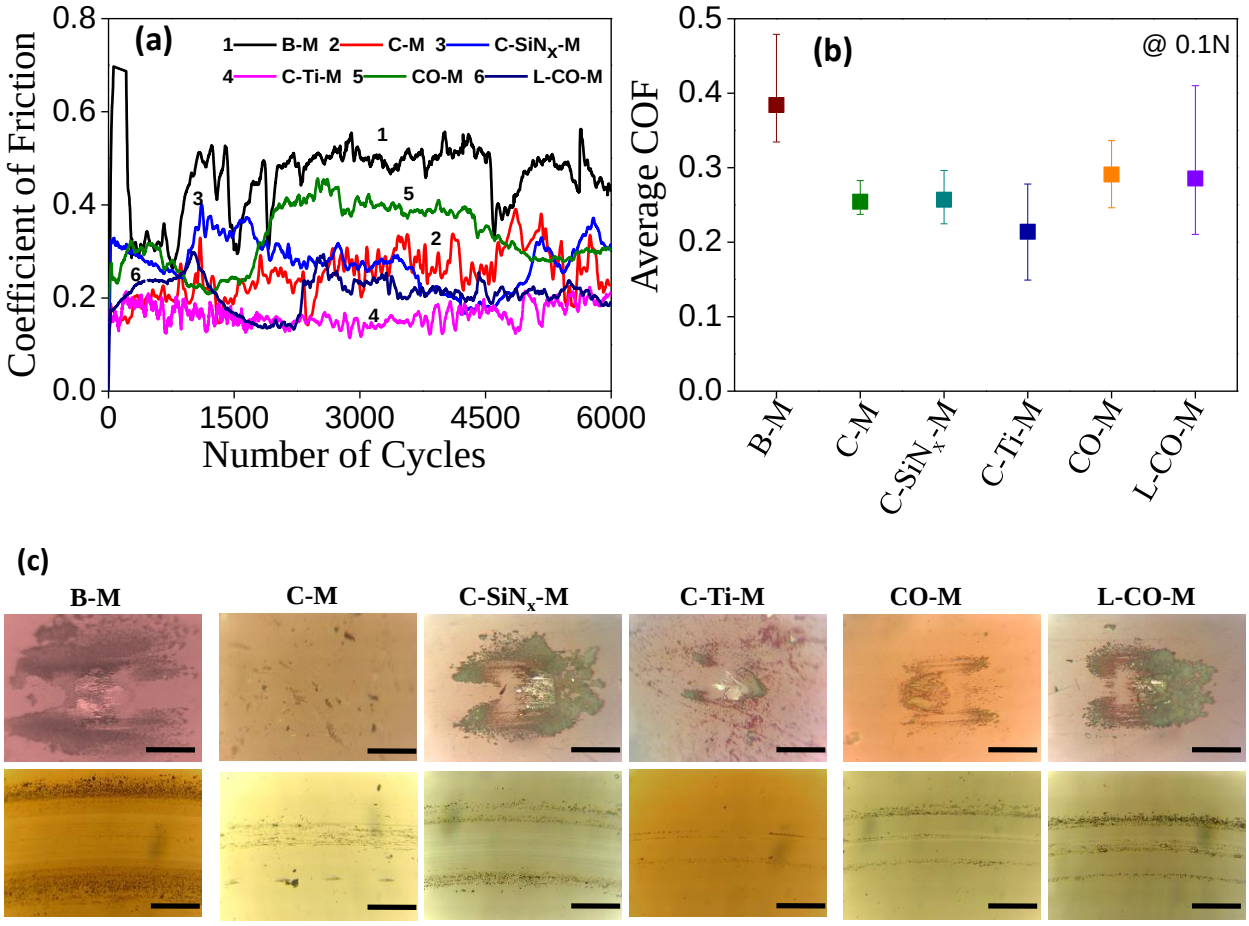

Figure 2: (a) Frictional curves for various samples after 6000 cycles of sliding against a sapphire (Al_2O_3) ball at a normal load of 0.1 N. (b) Average COF values based on three to four measurements of each sample. (c) Optical microscope images of the balls and wear tracks after the ball-on-disk tribological tests on the different samples. Scale bars in the optical microscope images represent 100 µm.

To understand the difference in the tribological performance of the overcoats, we performed a series of computational simulations and spectroscopic measurements. Our hypothesis was that both the carbon surface chemistry and interfacial chemistry played a major role in controlling the friction and wear. Firstly, transport and range of ions in matter (TRIM) Monte Carlo simulations were performed to probe the interaction of energetic carbon species (at 90 eV) with a bare cobalt platinum (CoPt) media substrate, as well as the CoPt media with an overlayer of Ti or SiN_x, to simulate the process of carbon deposition in the samples of C-M, C-Ti-M and C-SiN_x-M, respectively. We anticipated that the presence of the Ti and SiN_x interlayers could cause atomic mixing. Figures 3a-c show the volume of interaction of carbon with CoPt media, and CoPt media with SiN_x and Ti overlayers, respectively. For consistency, the HRTEM-measured thicknesses of SiN_x and Ti were used in the models for the TRIM simulations. Snapshots of the carbon interaction with the substrates were captured with increasing carbon thickness, at intervals of 4 Å up to the final thickness of the carbon layer (16 Å) is used as the final thickness of the carbon layer in the TRIM simulations), to reveal the dynamic nature of the interaction as the carbon film grew. To visualize the atomic interactions more clearly, ball models were prepared and are presented in Figures 3a-c. At the start of the growth process, interaction of carbon with bare CoPt promoted atomic mixing to a certain depth in CoPt, while some of the CoPt atoms may have simultaneously migrated to the surface of the growing carbon film (Figure 3a). At this stage, the migrated CoPt atoms are expected to be present in the atomically thin layer of carbon whereas a significant amount of the energetic carbon species gets accommodated in the top 1-2 nm region of the CoPt media. As the growth of the carbon layer continued, most of the incoming carbon species were able to penetrate the grown carbon layer and cause sub-surface growth, known as sub-plantation, which could induce densification of the film and promote the formation of sp^3 bonds in the carbon

network[37-39]. This is discussed in detail in the next section. In the presence of the SiN_x layer, the carbon species were extensively mixed with Si and N atoms within the SiN_x layer, while some of the Si and N atoms may have simultaneously migrated to the growing carbon layer region but close to the carbon/SiN_x interface (Figure 3b). This was also applicable for the case of the Ti layer (Figure 3c), where a highly mixed interface layer was formed as a consequence of atomic mixing with the energetic carbon species. These atomic interactions could result in the generation of various types of hybrid bonds and lead to the strengthening of the interface. Thus, the use of energetic (90 eV) carbon species promoted atomic mixing that could enhance the interfacial bonding, especially when SiN_x and Ti interlayers are introduced. At the same time, 90 eV ion energy of incoming carbon species could lead to sub-surface growth of the carbon layer, which could in turn generate a denser film and a higher degree of sp^3 bonding within the carbon layer (which is still an amorphous carbon layer comprising a mixture of sp^2 + sp^3 bonded carbon). However, since the thickness of carbon layer in these overcoats is ≤ 2 nm, the thickness of carbon layer will also affect the sp^3 bonding as explained in the 3-phase model by Dwivedi et al. [39]. The interaction of 90 eV carbon ions with bare CoPt and the CoPt with SiN_x and Ti interlayers is also presented in **Supplementary Movie (SM1)**.

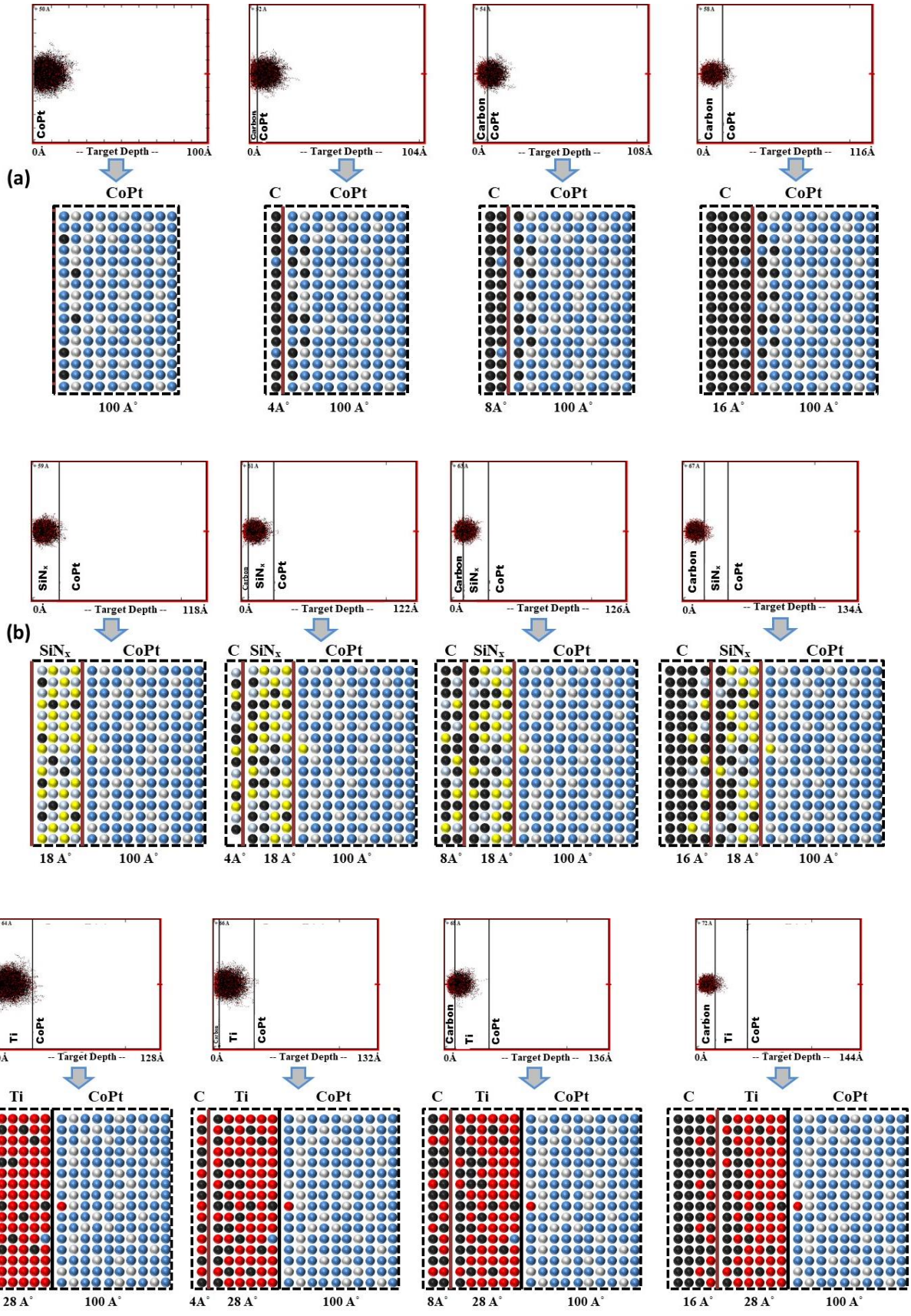
(a)
CoPt
0Å -- Target Depth -- 100Å
Carbon
CoPt
0Å -- Target Depth -- 104Å
Carbon
CoPt
0Å -- Target Depth -- 108Å
Carbon
CoPt
0Å -- Target Depth -- 116Å
CoPt
100 A˚
C CoPt
4A˚ 100 A˚
C CoPt
8A˚ 100 A˚
C CoPt
16 A˚ 100 A˚
(b)
SiNx
CoPt
0Å -- Target Depth -- 118Å
Carbon
SiNx
CoPt
0Å -- Target Depth -- 122Å
Carbon
SiNx
CoPt
0Å -- Target Depth -- 126Å
Carbon
SiNx
CoPt
0Å -- Target Depth -- 134Å
SiNx CoPt
18 A˚ 100 A˚
C SiNx CoPt
4A˚ 18 A˚ 100 A˚
C SiNx CoPt
8A˚ 18 A˚ 100 A˚
C SiNx CoPt
16 A˚ 18 A˚ 100 A˚
(c)
Ti
CoPt
0Å -- Target Depth -- 128Å
Carbon
Ti
CoPt
0Å -- Target Depth -- 132Å
Carbon
Ti
CoPt
0Å -- Target Depth -- 136Å
Carbon
Ti
CoPt
0Å -- Target Depth -- 144Å
Ti CoPt
28 A˚ 100 A˚
C Ti CoPt
4A˚ 28 A˚ 100 A˚
C Ti CoPt
8A˚ 28 A˚ 100 A˚
C Ti CoPt
16 A˚ 28 A˚ 100 A˚

Figure 3: TRIM simulations for atomic distribution resulting from surface bombardment by energetic species of carbon (at 90 eV), showing ball models and depth profile plots representing the (a) C-M, (b) C-SiN_x-M and (c) C-Ti-M samples. Snapshots of the simulations were taken at every 4 Å increase in the carbon layer thickness during the growth process, up to a final carbon layer thickness of 16 Å. The thicknesses of CoPt, SiN_x and Ti were set at 10 nm, 1.8 nm and 2.8 nm, respectively.

To experimentally confirm and validate the formation of various types of hybrid bonds at the interfaces (interface chemistry), and to quantify the sp^3 bonding content in the carbon layer (surface chemistry), XPS measurements were performed. The high-resolution C 1s spectra of monolithic carbon, bilayer overcoats and the commercial overcoat were deconvoluted into their constituent peaks after Shirley-background subtraction and are presented in Figures 4a-4d. Peak fitting was performed using Gaussian-Lorentzian components while fixing the peak positions of the same constituent peaks in different samples to precisely determine the bonding content. The C 1s spectra reveal the presence of sp^2C and sp^3C bonds along with the bonding of carbon with oxygen (C-O and C=O) [39]. An adventitious carbon peak (AC) was also included in all the spectra to consider the presence of environmental carbon on our samples[39]. Since our interest is on the sp^3C bonding that serves to enhance the density of the carbon overcoat, an area ratio method was performed to determine the sp^3 bonding content, as presented in Figure 4e. It is evident that the sp^3C bonding content in all the samples is less than 30%, and application of interlayers negligibly altered the amount of sp^3C bonding, although the C-Ti-M sample yielded the highest sp^3C bonding amongst all the samples. This is in agreement with the 3-phase model for the structure and bonding of ultrathin carbon films proposed by Dwivedi *et al.* [39] Another observation is that the sp^3C bonding content in our monolithic carbon and bilayer overcoats was found to be consistently higher than the commercial carbon overcoat in sample CO-M, as well as in carbon films of similar or higher thicknesses grown by low-energy deposition techniques such as sputtering where the

carbon species generally strike the substrate with energy ≤ 5 eV [37, 39]. Thus, the mixture of sp^3 and sp^2 bonded carbon present in the layer is different from conventional low-energy growth techniques, implying that there has been a modification in the amorphous carbon bonding with the use of the energetic (90 eV) carbon deposition process.

Further, to examine interface chemistry, the Si 2p (Figure 4f) and N 1s (Figure 4g) spectra of the C-SiN_x-M sample and the Ti $2p_{3/2}$ (Figure 4h) spectrum of the C-Ti-M sample were thoroughly investigated. The Si 2p spectrum revealed the presence of strong hybrid Si-C bonds due to the interaction of the energetic carbon from overcoat layer as well as from interatomic mixing with the SiN_x interlayer. This is in addition to intrinsic Si-N, Si-Si, and Si-O/Si-O-N bonds of the SiN_x layer. Likewise, the N 1s spectrum revealed newly generated hybrid bonds of (Cr/Co)-N, sp^3C-N/(Cr-Co)-N-O/Nitrile and sp^2C-N in addition to the intrinsic Si-N bonds. For the C-Ti-M sample, the Ti $2p_{3/2}$ spectrum (Figure 4h) revealed the presence of strong hybrid Ti-C bonds due to the interfacial interaction and interatomic mixing of carbon with the Ti interlayer, in addition to intrinsic Ti-Ti bonds. It has been proposed that Ti acts as an excellent transition/interlayer material for diamond-like carbon overcoats which enhances their adhesion and improves their functional properties [40-42]. Thus, in general, Ti and SiN_x induced hybrid bonds can enhance the interfacial strength and adhesion of the overcoats with the substrate, which is crucial for the wear resistance of the overcoats during contact sliding.

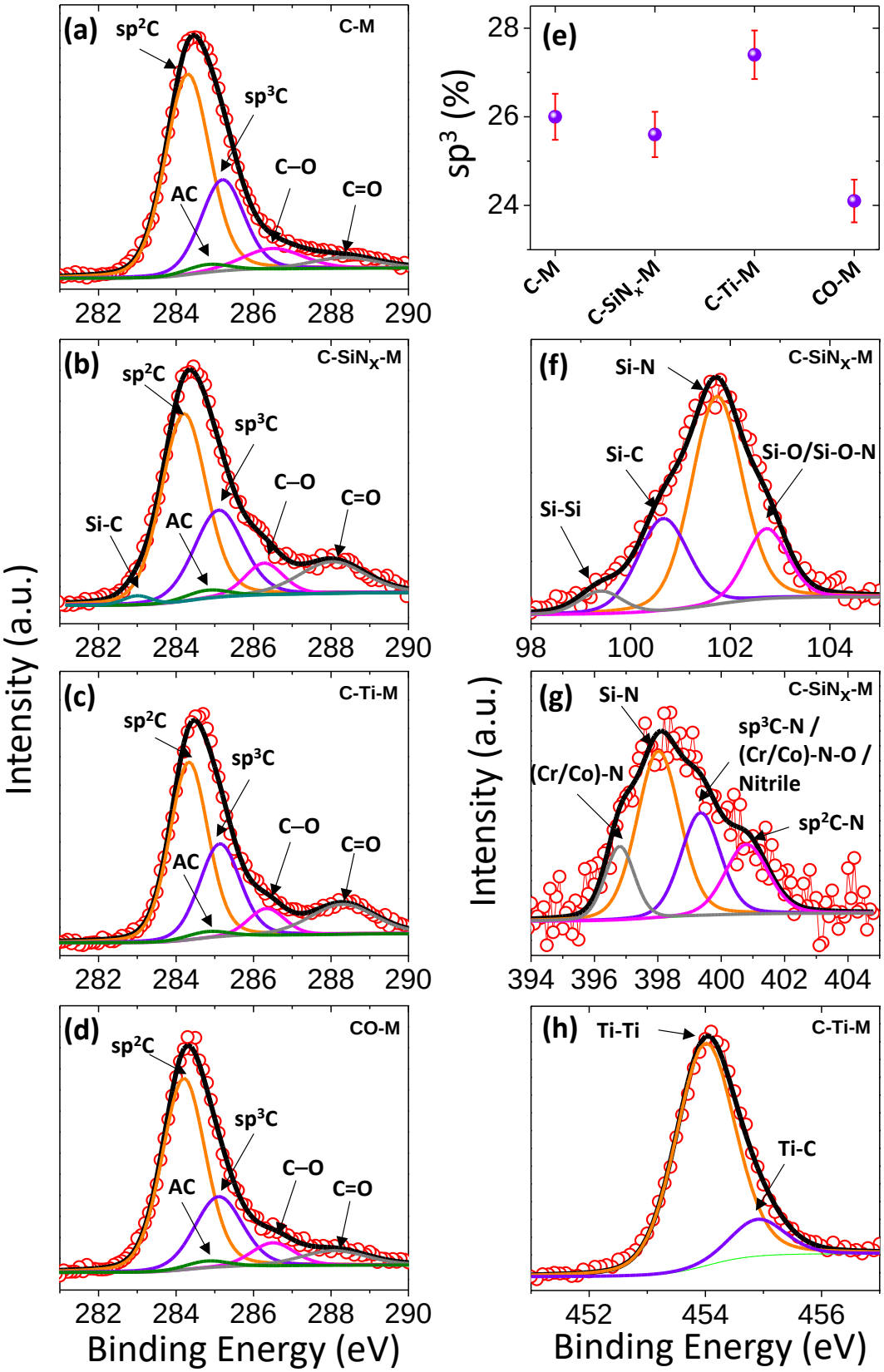
(a)
sp²C
C-M
sp³C
C–O
AC
C=O
282
284
286
288
290
(b)
C-SiNx-M
sp²C
sp³C
C–O
C=O
Si-C
AC
(c)
C-Ti-M
(d)
CO-M
Intensity (a.u.)
Binding Energy (eV)
(e)
sp³ (%)
28
26
24
C-M
C-SiNx-M
C-Ti-M
CO-M
(f)
Si-N
Si-C
Si-O/Si-O-N
Si-Si
98
100
102
104
(g)
sp³C-N /
(Cr/Co)-N-O /
Nitrile
(Cr/Co)-N
sp²C-N
394
396
398
400
402
404
(h)
Ti-Ti
Ti-C
452
454
456

Figure 4: Deconvoluted high resolution C 1s spectra of samples (a) C-M, (b) C-SiN_X-M, (c) C-Ti-M and (d) CO-M. (e) Variation of sp^3 carbon fraction for the different samples calculated by an area ratio method using the sp^3 carbon constituent peak. Deconvoluted high resolution spectra of (f) Si 2p for sample C-SiN_X-M, (g) N 1s for sample C-SiN_X-M, and (h) Ti 2p for sample C-Ti-M.

To get a better understanding about the wear resistance of the overcoats, we performed XPS measurements at various locations inside and outside of the wear track on a few important samples. High resolution XPS C 1s and Pt 4f spectra were recorded for samples C-M, C-SiN_x-M and C-Ti-M (Figure 5a-c). Additional high-resolution Si 2p and Ti 2p spectra were also recorded concurrently for samples C-SiN_x-M and C-Ti-M, respectively. In Figure 5a-5c, locations labelled with the letter O (O_1-O_2) denote the spectra recorded at locations outside of the wear track, whereas locations labelled with the letter T (T_1-T_4) denote the spectra recorded at locations inside the wear track. We found that carbon was still present at all locations inside the wear track (T_1-T_4) for sample C-M (Figure 5a), although the intensity of carbon was significantly reduced with respect to the C 1s spectra recorded from outside of the wear track locations (O_1-O_2). In the C-SiN_x-M sample (Figure 5b), there was also a reduction in the intensity of the carbon peak at the wear track locations (T_1-T_4) with respect to C 1s spectra recorded outside of the wear track (O_1-O_2). At the same time, the presence of the Si peak in the Si 2p spectra from the wear track locations T_1-T_4 also confirmed that SiN_x still remained on the wear track after the tribological test. Likewise, in the C-Ti-M sample (Figure 5c), we observed the presence of carbon as well as Ti on the wear track locations T_1-T_4 based on their respective peaks in the C 1s and Ti 2p spectra. Compared with the C-M and C-SiN_x-M samples, the intensity of the C 1s peak on the wear track in C-Ti-M was not much reduced with respect to the C 1s peak recorded outside of the wear track. These results indicate that among the three samples, the resistance of the overcoat to sliding wear (at 0.1 N normal load) was highest in C-Ti-M.

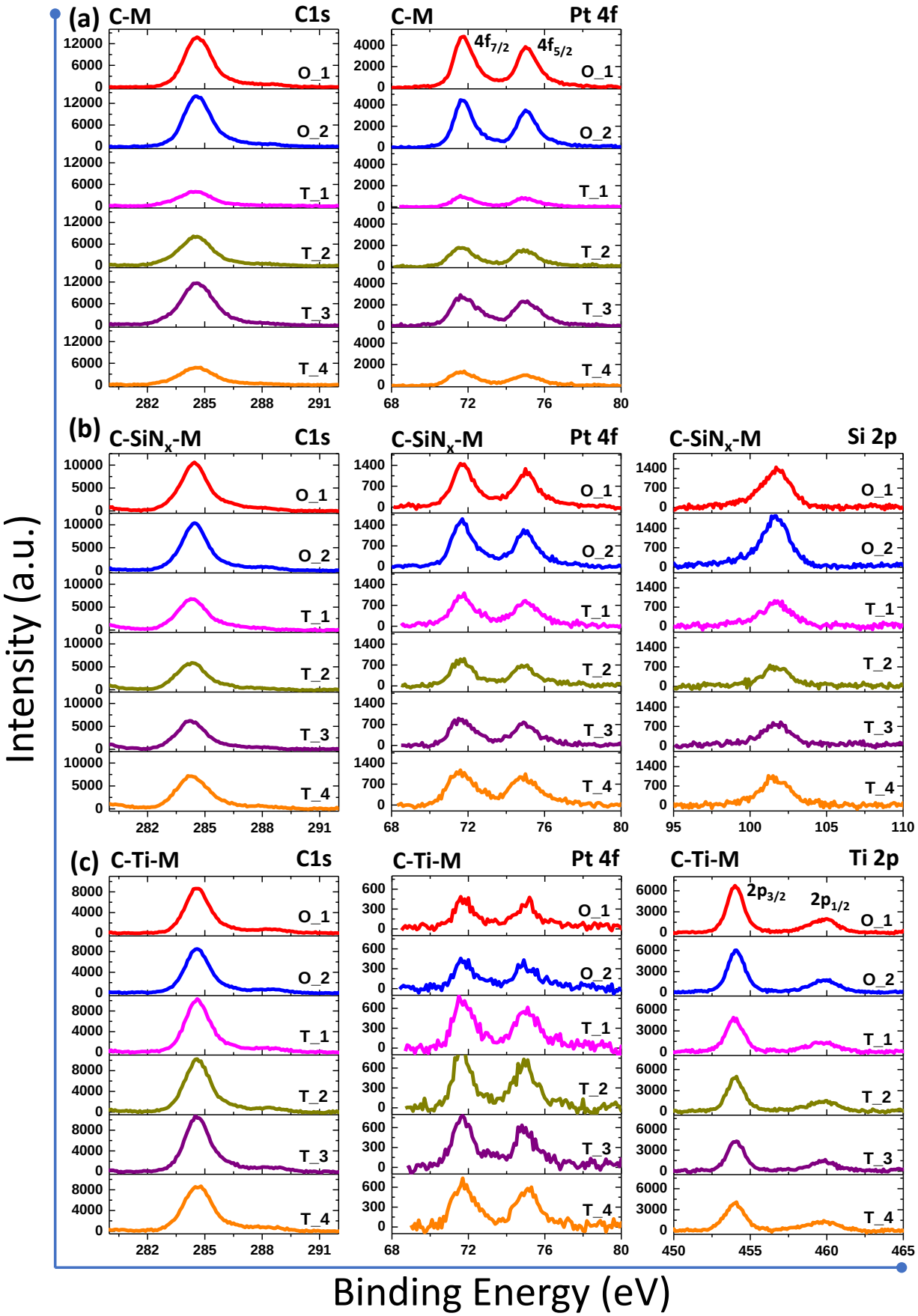
(a) C-M C1s
C-M Pt 4f
4f7/2
4f5/2
(b) C-SiNx-M C1s
C-SiNx-M Pt 4f
C-SiNx-M Si 2p
(c) C-Ti-M C1s
C-Ti-M Pt 4f
C-Ti-M Ti 2p
2p3/2
2p1/2
O_1
O_2
T_1
T_2
T_3
T_4
Intensity (a.u.)
Binding Energy (eV)

Figure 5: XPS high resolution spectra recorded on samples C-M, C-SiN_x-M and C-Ti-M at various locations outside of the wear track (locations O_1 and O_2) and inside the wear track (locations T_1, T_2, T_3 and T_4). (a) C 1s and Pt 4f spectra on sample C-M, (b) C 1s, Pt 4f and Si 2p spectra on sample C-SiN_x-M and (c) C 1s, Pt 4f and Ti 2p spectra on sample C-Ti-M. The overcoat materials, *viz.* carbon in sample C-M, carbon and silicon (from SiN_x) in sample C-SiN_x-M and carbon and titanium in sample C-Ti-M was found to be present on wear track.

We now discuss the friction and wear mechanisms arising from the tribological tests. Graphitic carbon and highly sp^2 bonded carbon materials generally show low friction due to the low shear strength between the graphitic sp^2 layers, as the layers are held together by weak van der Waals interactions[1]. Moreover, in humid environments, water may intercalate in between the graphitic layers and further weaken these interactions, resulting in decreased friction [1, 3, 43, 44]. This was also found to occur in non-hydrogenated amorphous carbon films [44]. On the other hand, diamond and other highly sp^3 bonded carbon materials show high wear resistance due to their high hardness and density[3, 45]. Non-hydrogenated diamond-like carbon materials can also exhibit low friction in certain specific conditions such as high humidity where their surfaces are always passivated with H/OH moieties[3, 45]. In our case, we have deposited the ultrathin carbon overcoat layer at 90 eV. Generally, amorphous carbon films grown at an energy range of 50-90 eV possess very high ~ 70-90% sp^3 bonding and a correspondingly small amount of sp^2 bonding, and are normally referred to as tetrahedral amorphous carbon (ta-C). The generation of sp^3 bonds is achieved *via* a sub-plantation mechanism where the arriving carbon ions penetrate the grown carbon surface, and grow sub-surface leading to densification of the carbon layer [14, 37]. However, unlike traditional ta-C films, our carbon films possess a maximum of 25-28% sp^3 carbon bonding based on the XPS analysis. Actually, when the films are in the ultrathin regime of a few nanometers, the thickness of the film plays a big role in controlling the sp^2 and sp^3 carbon bonding [39] because the tuning of carbon bonding is expressed in view of 3-layer model concept (interface

layer, middle layer and surface layer) within the single carbon layer, as highlighted by Dwivedi *et al.* recently [39]. In such a circumstance, the sp^3 bonding is governed by the thickness of the bulk (or middle) layer/region of the carbon film with respect to the surface and interface regions (*i.e.*, the regions of the carbon film adjacent to the surface and substrate, respectively). This is because the surface and interface regions are generally rich in sp^2-bonded carbon (and remain almost constant for different overall thicknesses), whereas the middle region of the carbon film is the region that is rich in sp^3-bonded carbon which grows with increasing overall thickness of the carbon in ultrathin thickness regime [39]. Thus, due to ultralow thickness (~ 2 nm or less) of the carbon layer in both the monolithic and bilayer overcoat configurations, the middle region of the carbon layer is very small, hence explaining the relatively lower sp^3 carbon bonding content of 25-28% realized in these monolithic and bilayer overcoats with respect to conventional (thicker) ta-C films. Nonetheless, the carbon network still possesses sufficient sp^3 bonding to maintain/improve the wear resistance during the tribological tests as compared to commercially grown carbon overcoats, due to the excellent load-bearing capability of the sp^3 carbon phase. Conversely, the friction reduction in the monolithic carbon sample C-M and bilayer overcoat samples C-SiN_x-M and C-Ti-M is mainly attributed to the surface region of the carbon layer that is rich in sp^2 carbon. The relatively lower friction could also have contributed in curbing the sliding wear, resulting in the improved wear resistance of the overcoats. Interestingly, the C-Ti-M overcoat yielded the best wear resistance when the measurements were performed at low load of 0.1 N. Since the sp^3 bonding in samples C-M and C-Ti-M is similar, the enhanced interfacial chemistry in terms of the generation of hybrid chemical bonds such as Ti-C is the main factor that distinguishes the two samples, and therefore explains why the C/Ti bilayer outperformed the monolithic carbon overcoat in terms of the wear resistance. However, the C/SiN_x bilayer overcoat (sample C-SiN_x-M) could

not yield a better wear resistance than the monolithic carbon overcoat in sample C-M when the tests were conducted at 0.1 N load. This may be due to the fact that once the sample starts to slide, the initial wear rate of the carbon could be slightly higher than in C-Ti-M or C-M. This is also supported based on the extent of wear debris that was transferred to the ball. As predicted and depicted in TRIM simulations and models, it is likely that some Si and N atoms from SiN_x had migrated into the carbon layer during the growth process), thus some of the underlying SiN_x could have been exposed to the ball counterface during the early sliding cycles. Si or SiN_x materials are tribologically-inferior since they readily oxidize to form abrasive oxides (SiO_x) [8]. These locations can cause more wear, and hence a relatively inferior wear resistance is observed in C-SiN_x-M. Now we focus on how do monolithic and bilayer carbon overcoats maintain a lower friction than bare media until the completion of tribological tests. When the carbon overcoat and ball tribo-pair is in sliding contact, wear is initiated in the early cycles and carbon-rich debris (mainly sp^2 rich carbon) is transferred to the counterface [46-48]. So, within the initial few to lower tens of cycles of the test, the tribological contacts quickly change from Media-Carbon/Al_2O_3 ball (or Media-Interlayer-Carbon/Al_2O_3 ball) to Media-Carbon/Carbon-Al_2O_3 ball (or Media-Interlayer-Carbon/Carbon-Al_2O_3 ball). Thus, sliding of the carbon-rich surface layer of the sample against the carbon-rich debris on the ball helps to maintain a relatively lower friction throughout the tribological test in most of the overcoats containing a carbon surface layer. From XPS analyses (Figure 5a-5c), we found traces of the overcoat materials on the wear tracks, namely carbon in sample C-M, carbon and silicon in sample C-SiN_x-M, and carbon and titanium in sample C-Ti-M, which helped to maintain low friction and wear of the overcoated samples with respect to bare media sample B-M.

Next, we investigated the friction and wear behavior of these overcoats in a more rigorous tribological environment. Firstly, we increased the normal load to 3 N, which is 30 times higher than the normal load of 0.1 N used in Figure 2, and kept the other tribological conditions the same. Figures 6a-6c show the plots of the frictional curves, average COF and optical images for wear properties analysis of the samples, respectively, after tribological tests were carried out at a normal load of 3 N. As compared to the lower load of 0.1 N, the COF of B-M at the higher load of 3 N was marginally reduced but it experienced a massive amount of wear damage as confirmed by the intense and very wide wear track on the sample, together with a large wear scar on the ball. There could be a combination of adhesive and abrasive wear in this sample. The monolithic carbon overcoat in sample C-M also underwent very severe wear damage (intense and wide wear track and wide wear scar on the ball) and its COF was measured to be similar to the bare media sample B-M. This suggests that the monolithic ultrathin carbon overcoat of 2 nm did not offer any significant protection to the underlying media at a higher load, and even resulted in more wear debris than the bare media sample. At the normal load of 3 N, the carbon surface layer may have been rapidly worn out and therefore exposing the underlying metallic/magnetic media surface to the counterface, causing severe wear. The commercially grown carbon overcoat samples of CO-M and L-CO-M also revealed exceptionally high wear damage, and their average COF was measured to be ≥ 0.3. On the other hand, the bilayer overcoats gave the best tribological performance in terms of high wear resistance, as revealed by the relatively narrower and fainter wear tracks together with a smaller wear scar on the balls than the rest of the samples, even though their COF values were not significantly lower. Thus, this tribological investigation confirmed that under high normal load conditions, the durability of the bilayer overcoats is superior to a monolithic carbon overcoat structure as well as carbon overcoats grown by a less energetic

commercial process. The wear results also validated and emphasized that, in a more rigorous tribological environment, the enhanced interfacial strength and adhesion provided by hybrid bonding present in the bilayer samples is the major factor in enhancing the wear resistance, as the sp^3 carbon bonding content in the samples of C-M, C-Ti-M, and C-SiN_x-M are very close to each other.

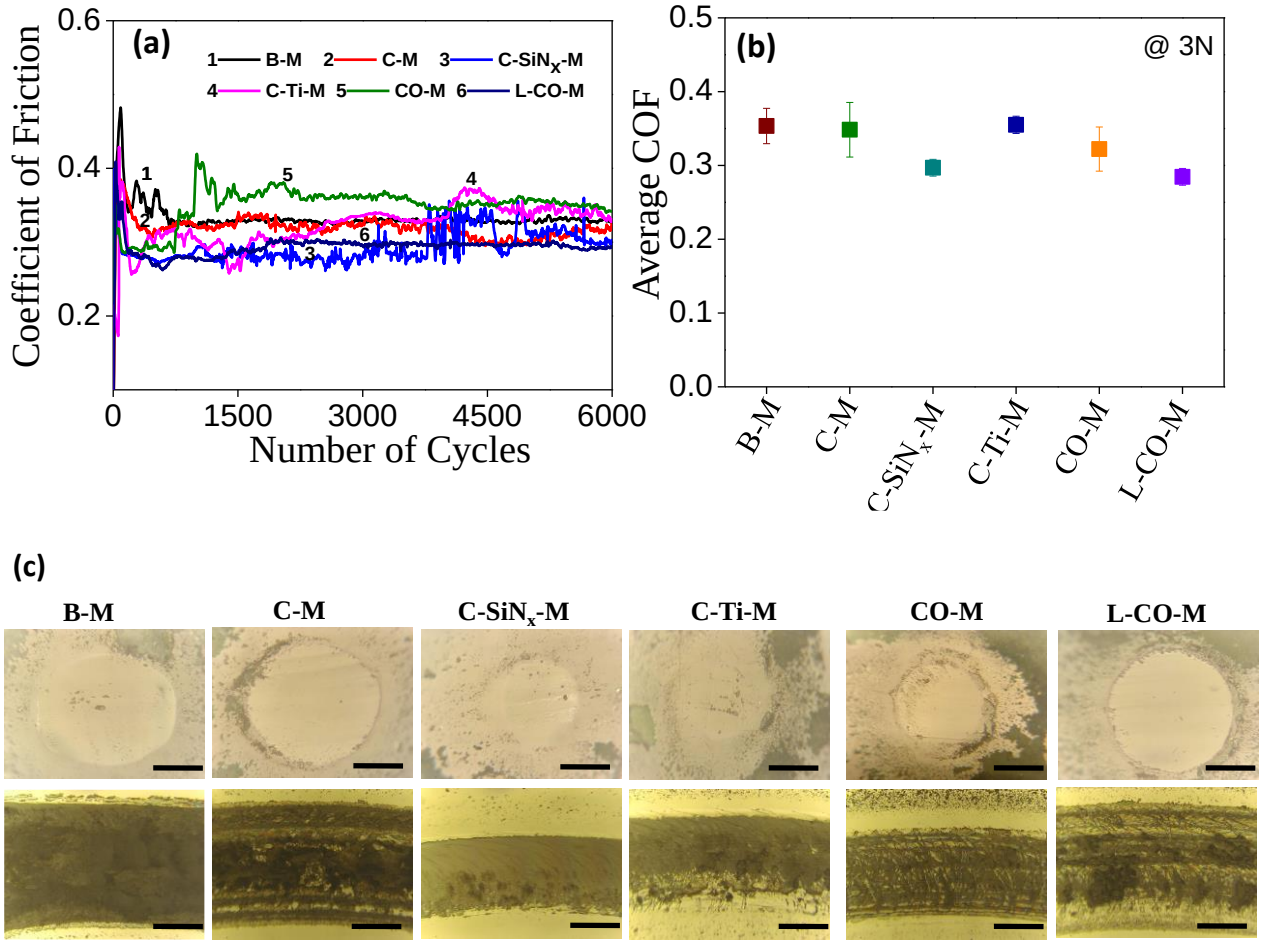

Figure 6: (a) Frictional curves after ball-on-disk tribological tests for bare media and media coated with different carbon-containing overcoats after 6000 cycles of sliding against a sapphire (Al_2O_3) ball at a higher normal load of 3N. (b) Average COF values and their corresponding standard deviations based on two to three measurements of each sample. (c) Optical microscope images of the balls (top) and wear tracks (bottom) after ball-on-disk tribological tests on the different samples. Scale bars in the optical microscope images represent 100 µm. Measurements were repeated on 2-3 pieces of each sample for consistency.

While there is clear evidence for the significant improvement of wear resistance when using bilayer overcoats in rigorous tribological environments, the sliding friction of the overcoats is yet to be minimized in such environments. This would be desirable for many applications that require high lubricity in addition to high wear durability, such as in the manufacturing and automotive industry. Recently, due to their low COFs during sliding, graphene-based materials have attracted attention for controlling sliding friction [1, 2, 49]. Hence, we have explored modifying the surfaces of all the samples (monolithic carbon, bilayer and commercially grown overcoats) with a layer of multilayer graphene (G) flakes by spin coating a solution of the flakes on top of the overcoats. The same was also applied on bare HD media to be used as a reference. Figure 7a shows the Raman spectra of G flakes modified samples. The Raman spectra clearly reveal the characteristic G and 2D peaks of multilayer graphene, suggesting the presence of multilayer graphene on all the samples. In addition to G and 2D peaks, all the multilayer graphene modified samples also revealed the D peak, indicating the presence of disorder in ring-like network of graphene. The G peak for graphene and graphitic materials corresponds to E_{2g} mode and is originated due to bond-stretching motion of pair of sp^2 carbon atoms in rings [2, 50, 51]. Whereas 2D peak is the second order overtone peak of D peak but unlike the D peak it does not require defects for its activation [51]. The 2D peak originates due to two phonon processes. The morphology of G flakes was also studied using FESEM (Figure 8a) and HRTEM (Figure 8b). The FESEM image (Figure 8a) indicates that the sheet-like G flakes are distributed throughout the sample which is further supported by HRTEM image (Figures 8b) that also distinctly reveal the transparent sheet-like morphology of G flakes. Further, selected area electron diffraction (SAED) measurement (Figure 8c) confirmed the multilayer structure of graphene which has a poly-crystalline nature.

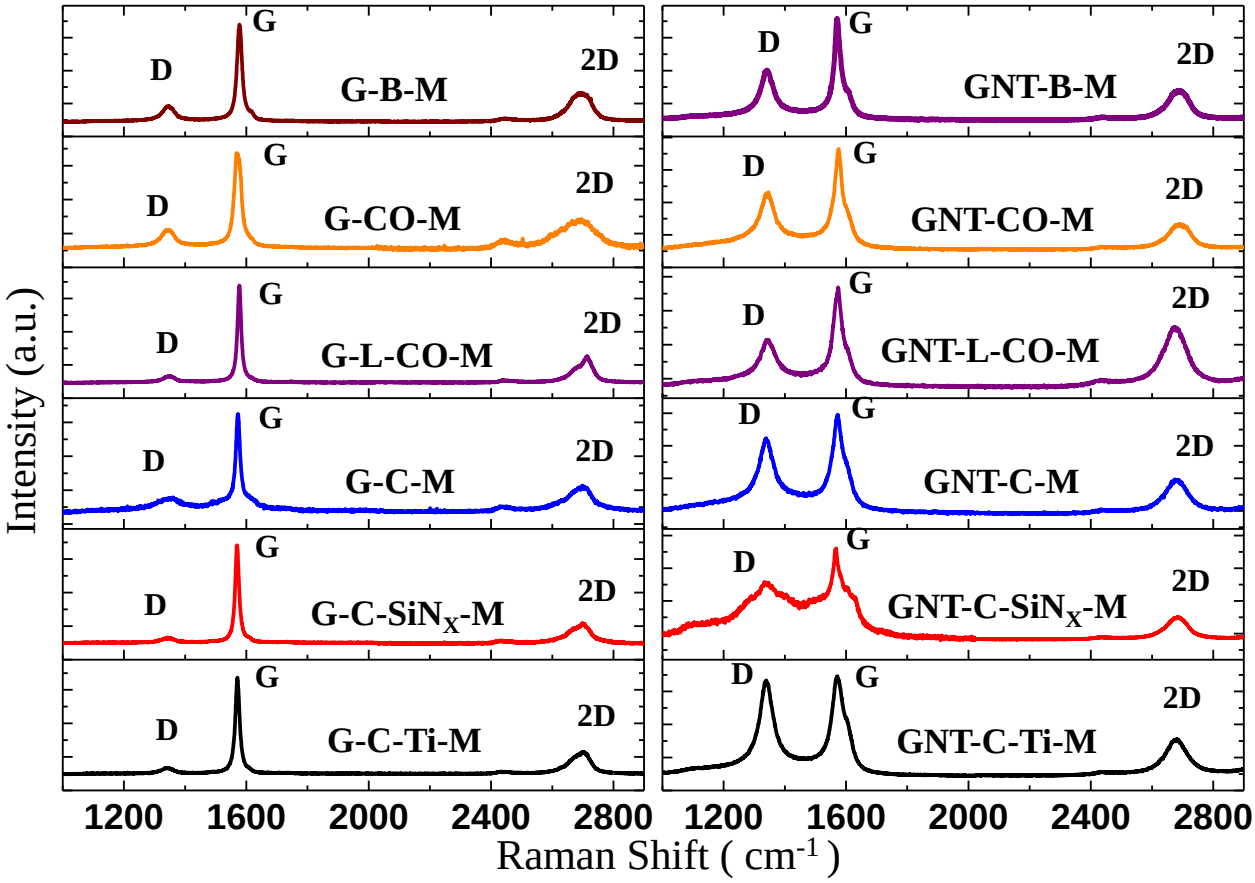

Figure 7: Raman spectra of (a) G layer and (b) composite GNT layer coated diverse samples.

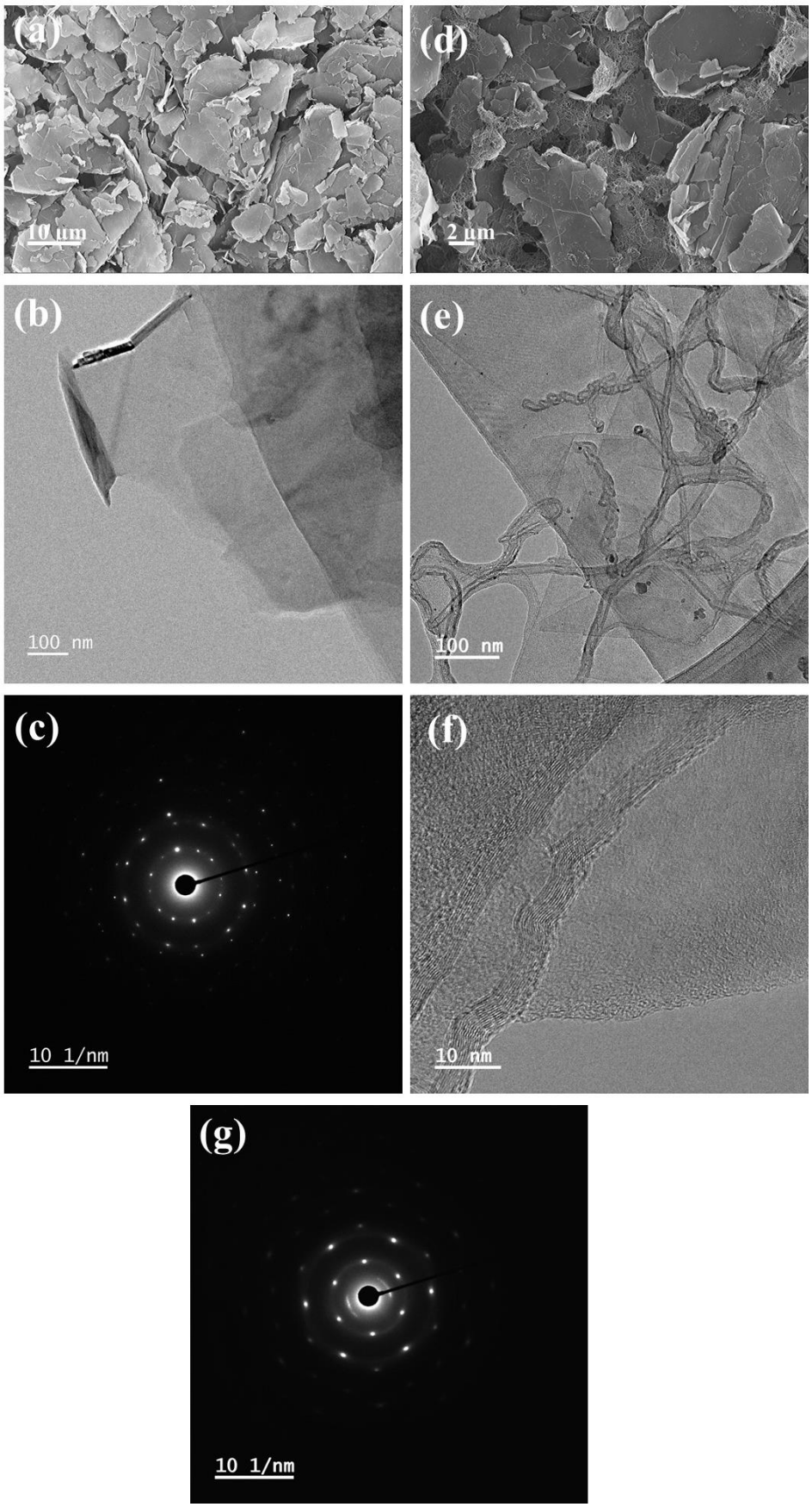
(a)
10 μm
(d)
2 μm
(b)
100 nm
(e)
100 nm
(c)
10 1/nm
(f)
10 nm
(g)
10 1/nm

Figure 8: (a) FESEM and (b) HRTEM Image and (c) SAED pattern of G flakes which are applied on diverse surfaces. (d) FESEM, (e) low resolution TEM, (f) high resolution TEM images and (g) SAED pattern of GNT composites which are applied on diverse surfaces.

Further, Figures 9a-9c show plots of the frictional curves, average COF and optical images for wear properties analysis of the G flakes modified samples, respectively, after tribological tests were carried out at a normal load of 3 N. Application of the G flakes was found to have negligibly altered the friction (Figures 9a and 9b) but slightly enhanced the wear of all the samples (Figure 9c). This led us to further explore other types of materials that could be used to modify the overcoat surfaces to simultaneously achieve slippery and wear resistant surfaces. We eventually developed a composite GNT coating which includes multilayer graphene + multiwall carbon nanotubes, in a 1:1 ratio, which were applied onto all the sample surfaces by spin coating from solution. The multiwall carbon nanotubes are cylinders of sp^2 carbon material which are stacked one another by weak van der Waals interaction. Thus, this material is not only having low shear strength but also holds unique cylindrical morphology which in collaboration with sheet-like G flakes can enable more slippery surfaces. Raman spectra (Figure 7b) confirm that the GNT composite layer is present on diverse samples as the characteristics G and 2D peaks with disorder D peak are appeared from all the sample surfaces. The FESEM images (Figure 8d) shows the CNT cylinders are muffled between the graphene sheets and with each other which may enable the sliding easier at the tribo-interface. The same observation is more obvious by HRTEM images (Figures 8e and 8f) that display the composite of G+CNT (forming GNT composite layer). SAED pattern (Figure 8g) shows the modification of crystallinity and crystal structure of the starting materials in the GNT composite. Through the SAED pattern, the typical six-fold intense reflections indicate the

multilayer nature of graphene in the GNT composite provide information about SAED pattern with bright circular rings revealed the crystalline nature and multilayer nature of GNT.

Figures 10a-10c show the plots of the frictional curves, average COF and optical images for wear properties analysis of the GNT modified samples, respectively, after tribological tests were carried out at a normal load of 3 N. It is evident from Figure 10a that the application of the composite GNT layer considerably reduced the friction of most of the samples in initial cycles. But when evaluating the average COF, the C/SiN_x and C/Ti bilayer overcoats modified with the composite GNT film yielded the best performance in terms of relatively lower friction than the GNT modified bare HD media, monolithic carbon overcoat and commercially grown carbon overcoat samples. We thoroughly probed the wear track using Raman spectroscopy to get a deeper insight into the GNT-induced modulation of sliding friction and wear. Figures 11a-11f show the Raman spectra recorded across the various locations on the wear track for GNT coated samples. It is evident that the characteristic D, G and 2D peaks of GNT are present at almost all locations measured on the wear tracks of samples GNT-L-CO-M, GNT-C-M, GNT-C-SiN_x-M and GNT-C-Ti-M with GNT-C-Ti-M, with a good intensity of peaks in all samples. In contrast, GNT was found to be present on only 1-2 locations for GNT-coated bare media (GNT-B-M) as well as GNT-coated commercial overcoat on media (GNT-CO-M). Correlating the Raman results to the tribological measurements, we see a strong correlation of the presence of GNT-like materials in helping to maintain the low friction and high frictional stability of the samples throughout the tribological tests. Hence the lesser amount of GNT on samples GNT-B-M and GNT-CO-M as a consequence of high wear and hence migration of constituent atoms from the wear track region could explain their relatively higher friction than the other samples. We now attempt to answer why do GNT composite layer favors to reduce the friction. The sheet-like G flakes and multiwall carbon

nanotube cylinders together make ensembles of GNT in which the cylinders can accommodate in between the G flakes or bottom and top of the G flakes. This largely reduces the sliding friction due to synergistic effect in terms of altering of the contact area, adhesion of tribo-pair and unique local contact point(s) at the tribo-interfaces (multi-asperity contacts) with minimal sliding resistance.

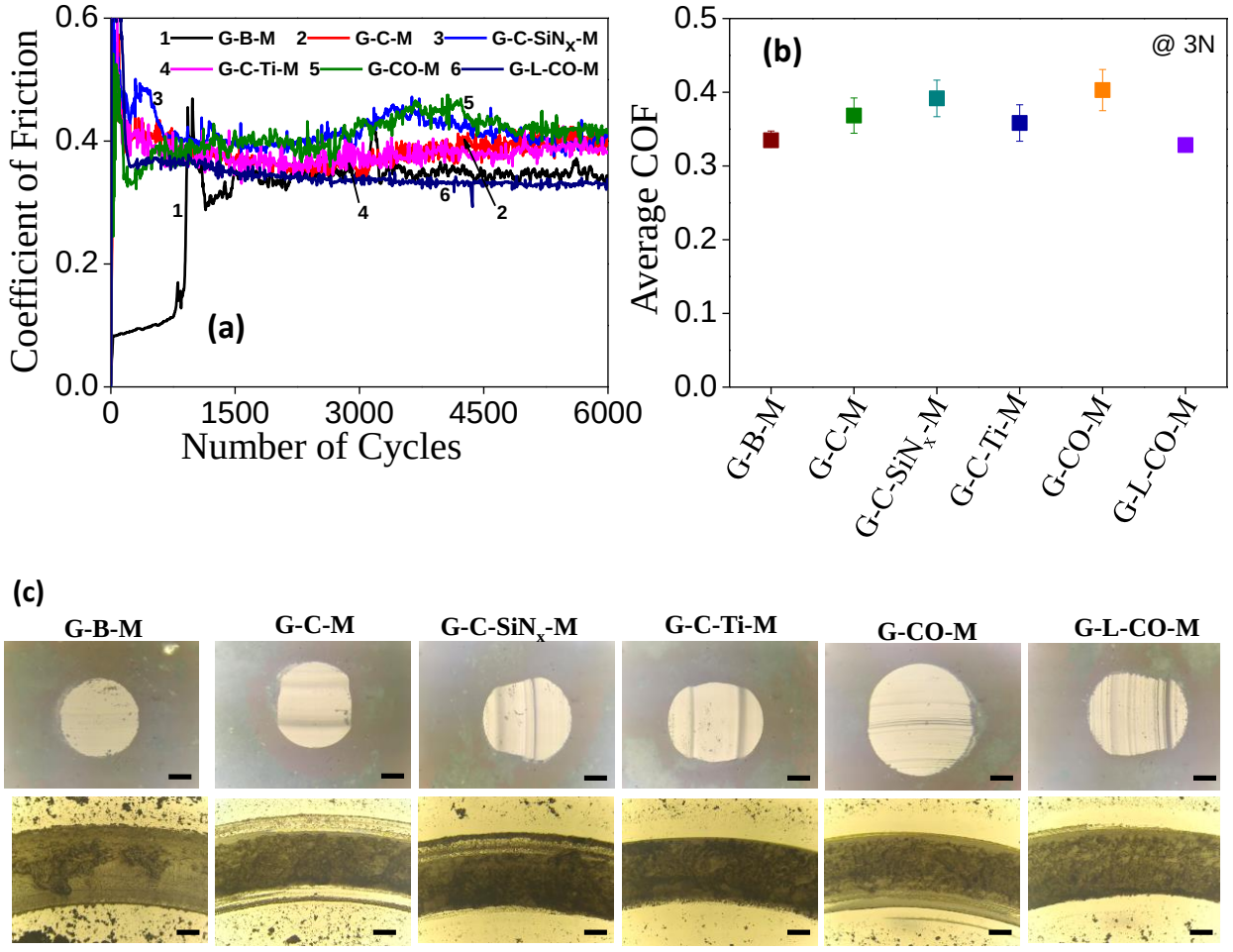

Figure 9: (a) Frictional curves of samples modified with a layer of multilayer graphene flakes after 6000 cycles of sliding against a sapphire (Al_2O_3) ball at a normal load of 3 N. (b) Average COF values and their corresponding standard deviations based on at least two to four measurements of each sample. (c) Optical microscope images of the balls (top) and wear tracks (bottom) after ball-on-disk tribological tests on the different samples. Scale bars in the optical microscope images represent 100 µm.

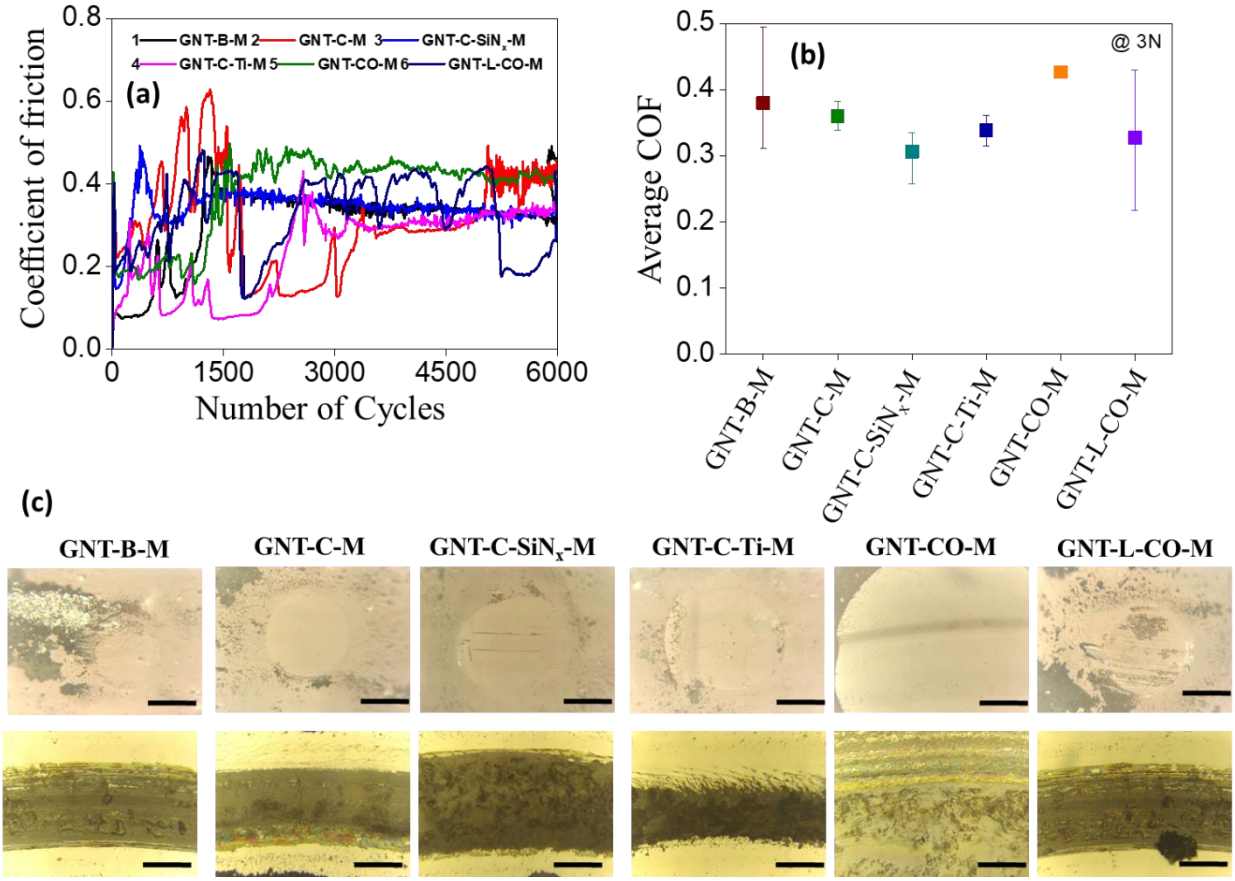

Figure 10: (a) Frictional curves after ball-on-disk tribological tests on samples modified with a GNT-coated layer after 6000 cycles of sliding against a sapphire (Al_2O_3) ball at a normal load of 3 N. (b) Average COF values and their corresponding standard deviations based on at least two to four measurements of each sample. (c) Optical microscope images of the balls (top) and wear tracks (bottom) after ball-on-disk tribological tests on the different samples. Scale bars in the optical microscope images represent 100 µm.

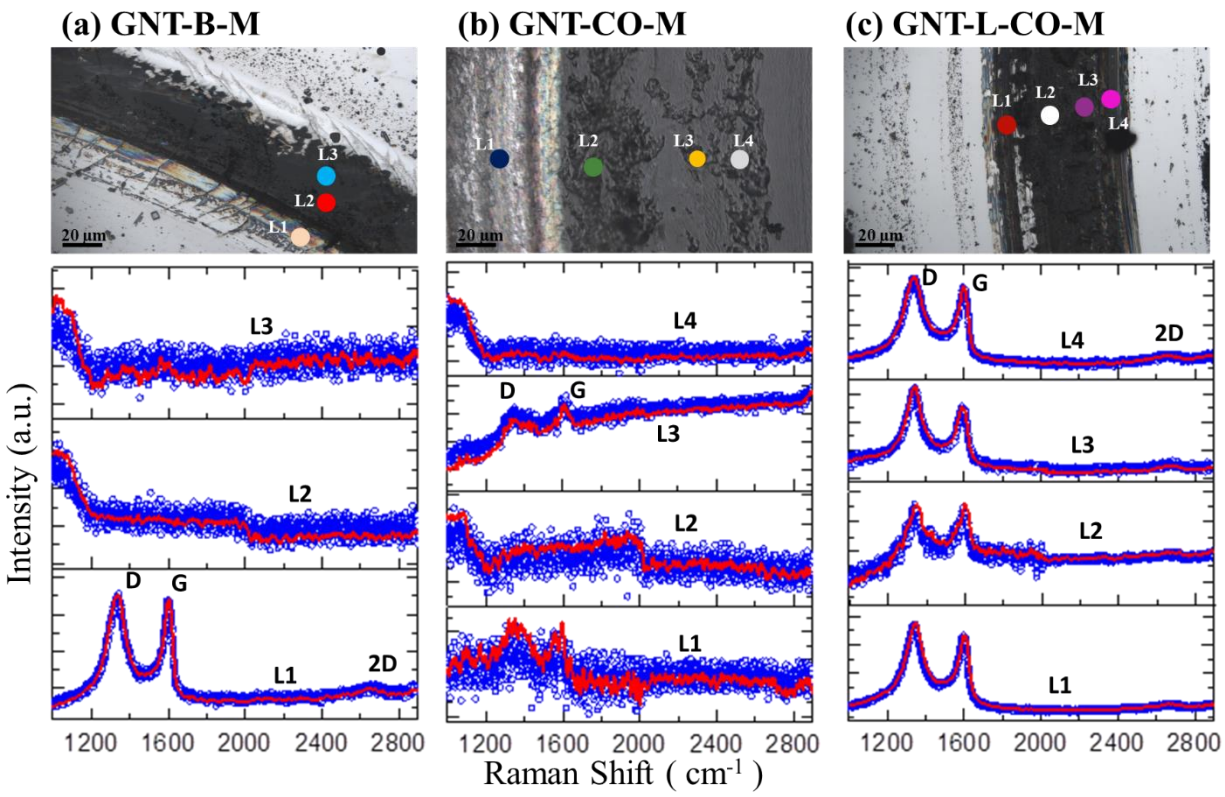
(a) GNT-B-M
(b) GNT-CO-M
(c) GNT-L-CO-M
L1
L2
L3
L4
20 μm
D
G
2D
Intensity (a.u.)
1200 1600 2000 2400 2800
Raman Shift (cm-1)

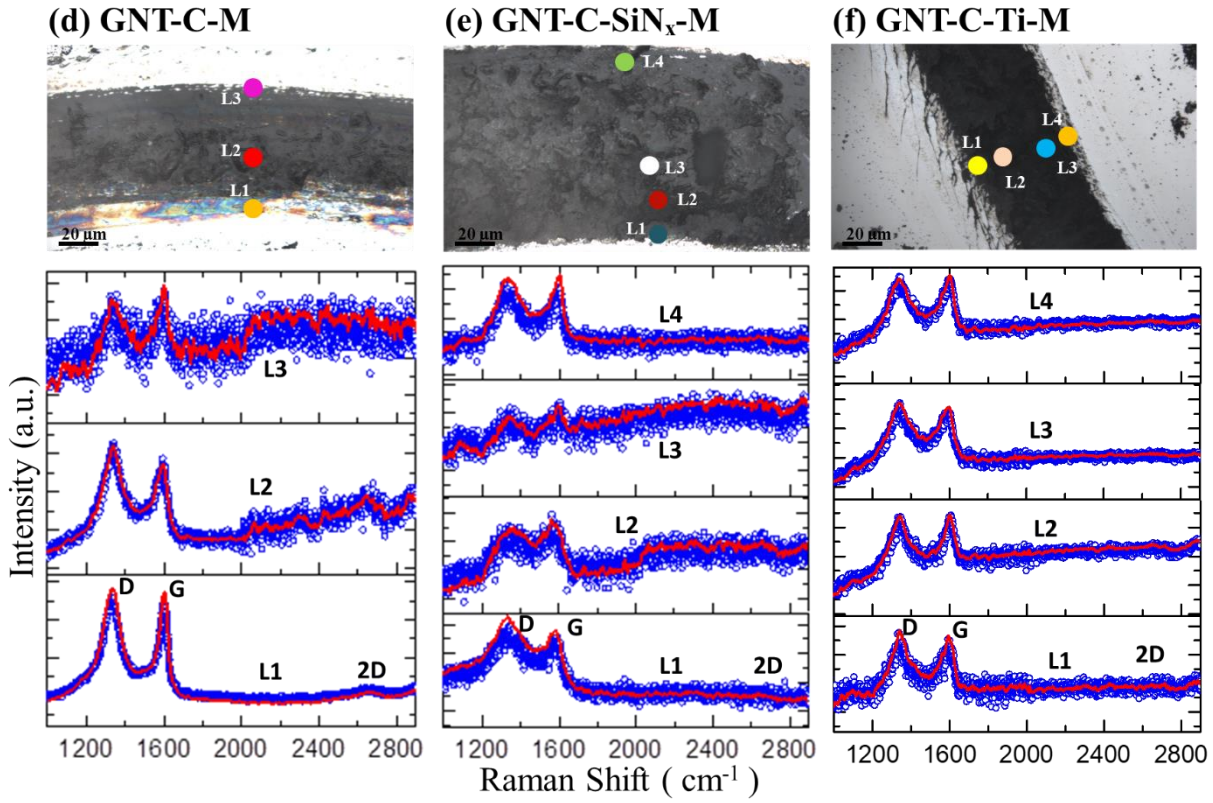
(d) GNT-C-M
(e) GNT-C-SiNx-M
(f) GNT-C-Ti-M
L1
L2
L3
L4
20 μm
D
G
2D
Intensity (a.u.)
1200 1600 2000 2400 2800
Raman Shift (cm-1)

Figure 11: Raman spectra for wear track analysis of GNT-coated samples: (a) GNT-B-M, (b) GNT-CO-M, (c) GNT-L-CO-M, (d) GNT-C-M, (e) GNT-C-SiN_x-M, and (f) GNT-Ti-M. Raman spectra recorded at different locations across the wear track (indicated by the yellow dots in the optical microscope images of the wear tracks).

To investigate another type of rigorous tribological environment, we looked at a longer sliding time by increasing the number of cycles to 30000 cycles, i.e. 5 times the normal test duration, while maintaining the normal load at 0.1 N. Since the C/Ti bilayer overcoat (sample C-Ti-M) yielded the best tribological performance in all of the previous tribological test environments, we were more interested in this sample for long-term tribological testing. Figure 12a shows the frictional curves of sample B-M and C-Ti-M measured for 30000 cycles, and their corresponding optical images for wear damage analysis are shown in Figure 12b. Bare media sample B-M showed a very high and fluctuating COF of ~ 0.6-0.8 throughout the completion of the test, and the optical images of the ball and wear track indicated very severe wear damage judging from the intensity and width of the wear track together with the large amount of debris transferred to the ball. Importantly, the C/Ti bilayer overcoat not only achieved a lower friction with a COF fluctuating between 0.2-0.4, but also attained excellent wear resistance with relatively faint wear track and less debris transfer to the ball than bare media, hence demonstrating the long-term wear durability of the C/Ti bilayer overcoat. We also investigated the tribological behavior of the C/Ti bilayer overcoat with its surface modified with multilayer G flakes and GNT for 30000 cycles. However, not much variation in friction and wear was observed between the surface modified and unmodified C/Ti bilayer overcoat samples. This suggests that for long-term contact sliding, the C/Ti bilayer overcoat itself is an excellent candidate for friction and wear reduction.

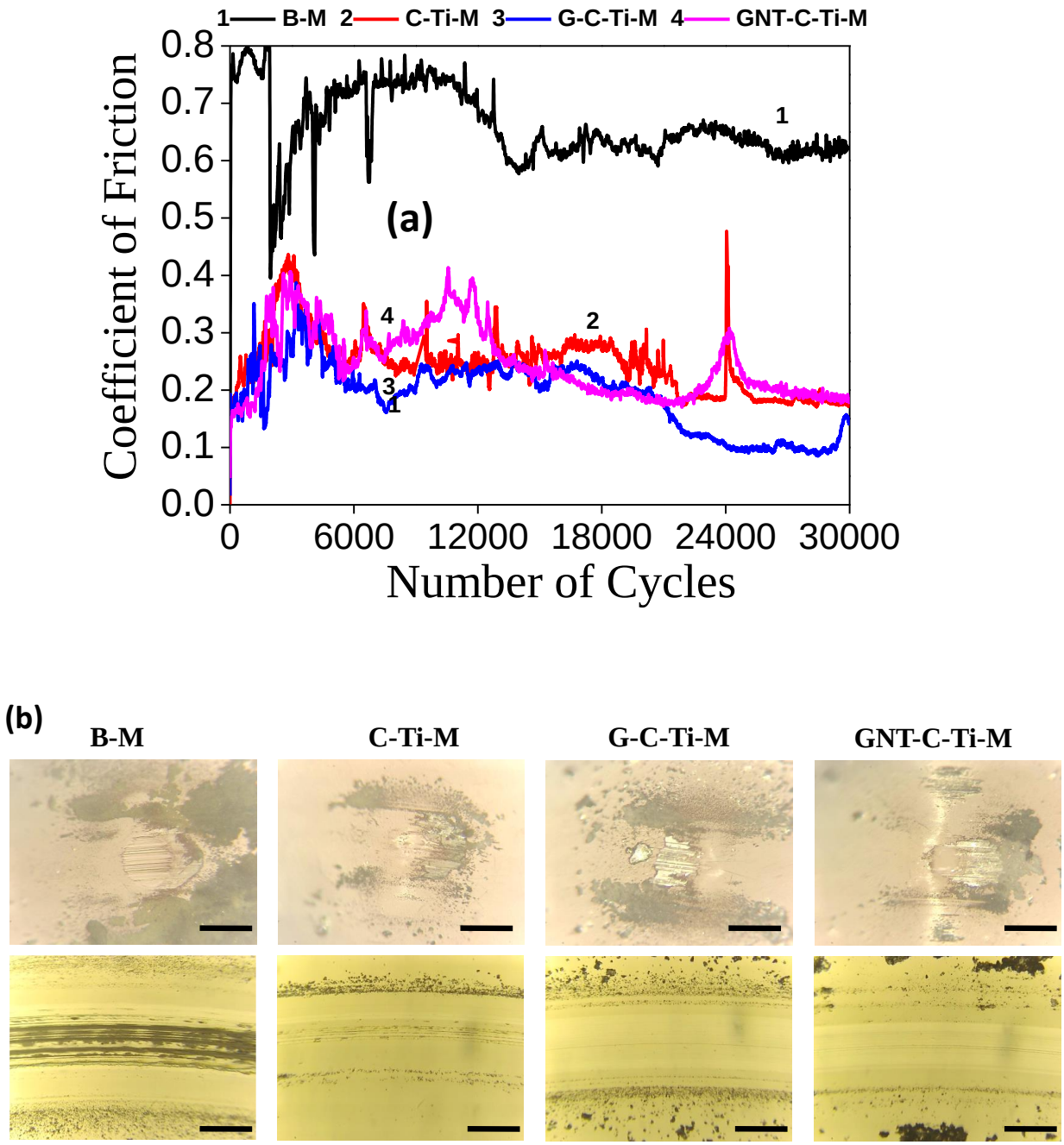

Figure 12: (a) Frictional curves of samples B-M, C-Ti-M, G-C-Ti-M, GNT-C-Ti-M after 30000 cycles of sliding against a sapphire (Al_2O_3) ball at a normal load of 0.1 N. (b) Optical microscope images of the balls (top) and wear tracks (bottom) after ball-on-disk tribological tests on the different samples. Scale bars in the optical microscope images represent 100 µm.

4. Conclusions

We have designed and developed 2-4.5 nm thick overcoats including monolithic carbon overcoats as well as C/Ti and C/SiN_x bilayer overcoats using an energetic deposition (@ 90 eV) for the carbon layer, for the purpose of reducing friction and wear in moving mechanical assemblies. When subjected to ball-on-disk tribological tests, the 2 nm thick monolithic carbon overcoat grown by the energetic deposition process outperformed relatively thicker commercially grown carbon overcoats with and without a lubricant layer, in terms of possessing lower friction and higher wear resistance. We have also observed that the C/Ti and C/SiN_x bilayer overcoats show excellent tribological performance in similar and more rigorous tribological test conditions. The energetic deposition process of carbon at 90 eV was found to be key to the improved tribological properties, due to extensive interatomic mixing between the carbon species and the substrate, coupled with the favorable energy for sp^3 carbon bond formation within the carbon layer. This resulted in enhanced interfacial strength and adhesion (strengthened interface chemistry), along with a mixed sp^3 and sp^2 bonded amorphous carbon overcoat with sufficient sp^3 bonding (unique carbon surface chemistry), which both contributed synergistically to achieving low friction and wear resistant surfaces. The best tribological performance was achieved in the C/Ti bilayer overcoats, and it is proposed that with further thickness engineering, the C/Ti bilayer overcoats could be explored for its implementation on hard disk media in functional HDDs for long-term protection. Finally, we found that the application of a spin-coated GNT composite layer on top of the carbon overcoat further added to the overcoat's lubricity and wear resistance.

Acknowledgements

The authors wish to thank Director, CSIR-AMPRI, Bhopal, India for his kind support. This research was supported by the Science and Engineering Research Board (SERB), India, under the project code SRG/2021/000105. R.K. acknowledges the Department of Science and Technology (DST), India for providing financial support through the DST INSPIRE (JRF) fellowship. Authors wish to thank Mr. Harish, Dr M. Ashiq, Dr M. Shafeeq, Mr. A. Khare, Dr P. Kumar, Dr Rajeev Kumar, and Dr D. P. Mondal from CSIR-AMPRI, Bhopal for their help. The TEM work was performed at Analytical HRTEM Laboratory, CSIR-AMPRI, Bhopal supported by CSIR under Facility Creation Project (MLP0110).

Authors contributions:

Rajesh Kumar: Designed the research project. Prepared the samples and performed the characterizations. Wrote the initial draft of the manuscript.

Pankaj Bharti: Helped in characterizations. Provided constructive inputs on experimental results analysis. Critically reviewed the manuscript and helped to improve the manuscript draft.

Chetna Dhand: Helped in characterizations. Provided constructive inputs on experimental results analysis. Critically reviewed the manuscript and helped to improve the manuscript draft.

Reuben J. Yeo: Helped in characterizations. Provided constructive inputs on experimental results analysis. Critically reviewed the manuscript and helped to improve the manuscript draft.

Mingsheng Zhang: Helped in characterizations. Provided constructive inputs on experimental results analysis.

Neeraj Dwivedi: Conceived the research idea. Designed the research project. Helped in characterizations. Provided constructive inputs on experimental results analysis. Critically reviewed the manuscript and helped to improve the manuscript draft.

Funding:

This research was supported by the Science and Engineering Research Board (SERB), India, under the project code SRG/2021/000105.

Conflict of Interest

The authors declare that they have no conflict of interest

Data Availability Statement

The data that support the findings of this study are available on request from the corresponding author.

References

[1] D. Berman, S.A. Deshmukh, S.K. Sankaranarayanan, A. Erdemir, A.V. Sumant, Macroscale superlubricity enabled by graphene nanoscroll formation, Science, 348 (2015) 1118-1122.
[2] N. Dwivedi, A. Ott, K. Sasikumar, C. Dou, R. Yeo, B. Narayanan, U. Sassi, D. De Fazio, G. Soavi, T. Dutta, Graphene overcoats for ultra-high storage density magnetic media, Nature communications, 12 (2021) 1-13.
[3] N. Dwivedi, R.J. Yeo, Z. Zhang, C. Dhand, S. Tripathy, C.S. Bhatia, Interface engineering and controlling the friction and wear of ultrathin carbon films: high sp3 versus high sp2 carbons, Advanced Functional Materials, 26 (2016) 1526-1542.

[4] W. Ye, M. Xie, Z. Huang, H. Wang, Q. Zhou, L. Wang, B. Chen, H. Wang, W. Liu, Microstructure and tribological properties of in-situ carbide/CoCrFeNiMn high entropy alloy composites synthesized by flake powder metallurgy, Tribology International, 181 (2023) 108295.
[5] D. Hua, X. Liu, W. Wang, Q. Zhou, Q. Xia, S. Li, J. Shi, H. Wang, Formation mechanism of hierarchical twins in the CoCrNi medium entropy alloy, Journal of Materials Science & Technology, 140 (2023) 19-32.
[6] K. Holmberg, A. Erdemir, Influence of tribology on global energy consumption, costs and emissions, Friction, 5 (2017) 263-284.
[7] N. Dwivedi, N. Satyanarayana, R.J. Yeo, H. Xu, K.P. Loh, S. Tripathy, C.S. Bhatia, Ultrathin carbon with interspersed graphene/fullerene-like nanostructures: a durable protective overcoat for high density magnetic storage, Scientific reports, 5 (2015) 1-16.
[8] R.J. Yeo, N. Dwivedi, E. Rismani, N. Satyanarayana, S. Kundu, P.S. Goohpattader, H. Tan, N. Srinivasan, B. Druz, S. Tripathy, Enhanced tribological, corrosion, and microstructural properties of an ultrathin (< 2 nm) silicon nitride/carbon bilayer overcoat for high density magnetic storage, ACS applied materials & interfaces, 6 (2014) 9376-9385.
[9] B. Marchon, T. Pitchford, Y.-T. Hsia, S. Gangopadhyay, The head-disk interface roadmap to an areal density of Tbit/in2, Advances in Tribology, 2013 (2013).
[10] N. Dwivedi, R.J. Yeo, L.J. Yak, N. Satyanarayana, C. Dhand, T.N. Bhat, Z. Zhang, S. Tripathy, C.S. Bhatia, Atomic scale interface manipulation, structural engineering, and their impact on ultrathin carbon films in controlling wear, friction, and corrosion, ACS applied materials & interfaces, 8 (2016) 17606-17621.
[11] R.L. Wallace Jr., The Reproduction of Magnetically Recorded Signals, Bell System Technical Journal, 30 (1951) 1145-1173.
[12] N. Dwivedi, A. Neogi, T.K. Patra, C. Dhand, T. Dutta, R.J. Yeo, R. Kumar, S. Hashmi, A. Srivastava, S. Tripathy, Angstrom-Scale Transparent Overcoats: Interfacial Nitrogen-Driven Atomic Intermingling Promotes Lubricity and Surface Protection of Ultrathin Carbon, Nano Letters, (2021).
[13] C. Casiraghi, A. Ferrari, R. Ohr, D. Chu, J. Robertson, Surface properties of ultra-thin tetrahedral amorphous carbon films for magnetic storage technology, Diamond and related materials, 13 (2004) 1416-1421.
[14] C. Casiraghi, J. Robertson, A.C. Ferrari, Diamond-like carbon for data and beer storage, Materials today, 10 (2007) 44-53.
[15] F. King, Datapoint thin film media, IEEE Transactions on Magnetics, 17 (1981) 1376-1379.
[16] S. Rajauria, O. Ruiz, S.V. Canchi, E. Schreck, Q. Dai, Electrostatically tunable adhesion in a high speed sliding interface, Physical review letters, 120 (2018) 026101.
[17] S. Wang, K. Komvopoulos, Structure evolution during deposition and thermal annealing of amorphous carbon ultrathin films investigated by molecular dynamics simulations, Scientific reports, 10 (2020) 1-12.
[18] P.M. Jones, J. Ahner, C.L. Platt, H. Tang, J. Hohlfeld, Understanding Disk Carbon Loss Kinetics for Heat Assisted Magnetic Recording, IEEE Transactions on Magnetics, 50 (2014) 144-147.
[19] F. Mangolini, F. Rose, J. Hilbert, R.W. Carpick, Thermally induced evolution of hydrogenated amorphous carbon, Applied Physics Letters, 103 (2013) 161605.
[20] N. Wang, K. Komvopoulos, F. Rose, B. Marchon, Structural stability of hydrogenated amorphous carbon overcoats used in heat-assisted magnetic recording investigated by rapid thermal annealing, Journal of Applied Physics, 113 (2013) 083517.
[21] B.K. Yen, R.L. White, R.J. Waltman, Q. Dai, D.C. Miller, A.J. Kellock, B. Marchon, P.H. Kasai, M.F. Toney, B.R. York, H. Deng, Q.-F. Xiao, V. Raman, Microstructure and properties of ultrathin amorphous silicon nitride protective coating, Journal of Vacuum Science & Technology A, 21 (2003) 1895-1904.
[22] F. Rose, D. Pocker, Q.-F. Xiao, V. Rawat, E. Brinkman, B. Marchon, Low surface energy and corrosion resistant ultrathin TiSiC disk overcoat, Journal of Applied Physics, 113 (2013) 213513.
[23] F. Rose, B. Marchon, V. Rawat, D. Pocker, Q.-F. Xiao, T. Iwasaki, Ultrathin TiSiN overcoat protection layer for magnetic media, Journal of Vacuum Science & Technology A, 29 (2011) 051502.

[24] W.-Y. Ding, J. Xu, W.-Q. Lu, X.-L. Deng, C. Dong, Ultra-thin α-SiNx protective overcoats for hard disks and read/write heads, Chinese Physics B, 18 (2009) 1570.
[25] D.J. Li, M.U. Guruz, C.S. Bhatia, Y.-W. Chung, Ultrathin CNx overcoats for 1 Tb/in.2 hard disk drive systems, Applied Physics Letters, 81 (2002) 1113-1115.
[26] T. Yamashita, G.L. Chen, J. Shir, T. Chen, Sputtered ZrO/sub 2/ overcoat with superior corrosion protection and mechanical performance in thin film rigid disk application, IEEE Transactions on Magnetics, 24 (1988) 2629-2634.
[27] A.H. Eltoukhy, A review of thin film media for magnetic recording, Journal of Vacuum Science & Technology A, 4 (1986) 539-542.
[28] K.M. Lee, C.D. Yeo, A.A. Polycarpou, Nanomechanical Property and Nanowear Measurements for Sub-10-nm Thick Films in Magnetic Storage, Experimental Mechanics, 47 (2007) 107-121.
[29] B.K. Yen, R.L. White, R.J. Waltman, C.M. Mate, Y. Sonobe, B. Marchon, Coverage and properties of a-SiNx hard disk overcoat, Journal of Applied Physics, 93 (2003) 8704-8706.
[30] P. Bernhard, C. Ziethen, R. Ohr, H. Hilgers, G. Schönhense, Investigations of the corrosion protection of ultrathin a-C and a-C:N overcoats for magnetic storage devices, Surface and Coatings Technology, 180-181 (2004) 621-626.
[31] W. Chatarat, N. Chanlek, C. Euaruksakul, H. Nakajima, J. Rusamiputi, S. Ittisanronnachai, N. Konkhunthot, S. Rujirawat, P. Songsiriritthigul, R. Yimnirun, Structural characterization of ultrathin diamond-like carbon overcoats for high areal density magnetic recording, Materialia, 27 (2023) 101650.
[32] N. Dwivedi, R.J. Yeo, C. Dhand, J. Risan, R. Nay, S. Tripathy, S. Rajauria, M.S. Saifullah, S.K. Sankaranarayanan, H. Yang, Boosting contact sliding and wear protection via atomic intermixing and tailoring of nanoscale interfaces, Science advances, 5 (2019) eaau7886.
[33] R.J. Yeo, N. Dwivedi, L. Zhang, Z. Zhang, C.Y. Lim, S. Tripathy, C.S. Bhatia, Superior wear resistance and low friction in hybrid ultrathin silicon nitride/carbon films: Synergy of the interfacial chemistry and carbon microstructure, Nanoscale, 9 (2017) 14937-14951.
[34] B.K. Gupta, B. Bhushan, Mechanical and tribological properties of hard carbon coatings for magnetic recording heads, Wear, 190 (1995) 110-122.
[35] B. Bhushan, G.S.A.M. Theunissen, X. Li, Tribological studies of chromium oxide films for magnetic recording applications, Thin Solid Films, 311 (1997) 67-80.
[36] R.J. Yeo, N. Dwivedi, L. Zhang, Z. Zhang, C.Y.H. Lim, S. Tripathy, C.S. Bhatia, Durable ultrathin silicon nitride/carbon bilayer overcoats for magnetic heads: The role of enhanced interfacial bonding, Journal of Applied Physics, 117 (2015) 045310.
[37] J. Robertson, Diamond-like amorphous carbon, Materials science and engineering: R: Reports, 37 (2002) 129-281.
[38] A. Ferrari, A. Libassi, B. Tanner, V. Stolojan, J. Yuan, L. Brown, S. Rodil, B. Kleinsorge, J. Robertson, Density, sp 3 fraction, and cross-sectional structure of amorphous carbon films determined by X-ray reflectivity and electron energy-loss spectroscopy, Physical Review B, 62 (2000) 11089.
[39] N. Dwivedi, R.J. Yeo, Z. Zhang, C. Dhand, S. Tripathy, C.S. Bhatia, Direct observation of thickness and foreign interlayer driven abrupt structural transformation in ultrathin carbon and hybrid silicon nitride/carbon films, Carbon, 115 (2017) 701-719.
[40] H. Cao, F. Qi, X. Ouyang, N. Zhao, Y. Zhou, B. Li, W. Luo, B. Liao, J. Luo, Effect of Ti transition layer thickness on the structure, mechanical and adhesion properties of Ti-DLC coatings on aluminum alloys, Materials, 11 (2018) 1742.
[41] K. Wang, H. Zhou, K. Zhang, X. Liu, X. Feng, Y. Zhang, G. Chen, Y. Zheng, Effects of Ti interlayer on adhesion property of DLC films: A first principle study, Diamond and Related Materials, 111 (2021) 108188.
[42] M. Zhang, T. Xie, X. Qian, Y. Zhu, X. Liu, Mechanical properties and biocompatibility of Ti-doped diamond-like carbon films, ACS omega, 5 (2020) 22772-22777.

[43] D. Berman, S.A. Deshmukh, S.K. Sankaranarayanan, A. Erdemir, A.V. Sumant, Extraordinary macroscale wear resistance of one atom thick graphene layer, Advanced Functional Materials, 24 (2014) 6640-6646.
[44] A. Erdemir, C. Donnet, Tribology of diamond-like carbon films: recent progress and future prospects, Journal of Physics D: Applied Physics, 39 (2006) R311.
[45] A.R. Konicek, D. Grierson, P. Gilbert, W. Sawyer, A. Sumant, R.W. Carpick, Origin of ultralow friction and wear in ultrananocrystalline diamond, Physical review letters, 100 (2008) 235502.
[46] T. Le Huu, H. Zaidi, D. Paulmier, P. Voumard, Transformation of sp3 to sp2 sites of diamond like carbon coatings during friction in vacuum and under water vapour environment, Thin Solid Films, 290 (1996) 126-130.
[47] A. Konicek, D. Grierson, A. Sumant, T. Friedmann, J. Sullivan, P. Gilbert, W. Sawyer, R.W. Carpick, Influence of surface passivation on the friction and wear behavior of ultrananocrystalline diamond and tetrahedral amorphous carbon thin films, Physical Review B, 85 (2012) 155448.
[48] N. Dwivedi, R.J. Yeo, H.R. Tan, R. Stangl, A.G. Aberle, C.S. Bhatia, A. Danner, B. Liao, Evidence for chemicals intermingling at Silicon/Titanium oxide (TiOx) interface and existence of multiple bonding states in monolithic TiOx, Advanced Functional Materials, 28 (2018) 1707018.
[49] C. Lee, Q. Li, W. Kalb, X.-Z. Liu, H. Berger, R.W. Carpick, J. Hone, Frictional characteristics of atomically thin sheets, science, 328 (2010) 76-80.
[50] N. Dwivedi, T. Patra, J.-B. Lee, R.J. Yeo, S. Srinivasan, T. Dutta, K. Sasikumar, C. Dhand, S. Tripathy, M.S. Saifullah, Slippery and Wear-Resistant Surfaces Enabled by Interface Engineered Graphene, Nano letters, 20 (2019) 905-917.
[51] A.C. Ferrari, J. Meyer, V. Scardaci, C. Casiraghi, M. Lazzeri, F. Mauri, S. Piscanec, D. Jiang, K. Novoselov, S. Roth, Raman spectrum of graphene and graphene layers, Physical review letters, 97 (2006) 187401.